Front. Chem. China 2011, 6(4): 310–331
DOI 10.1007/s11458-011-0251-8

REVIEW ARTICLE

Self-consistent field theory and its applications in polymer systems

Dadong YAN (✉)[1,2], Tongchuan SUO[2], Xinghua ZHANG[1,2], Xingkun MAN[2] and Bing MIAO[2]

This review article addresses the widely used self-consistent field theory (SCFT) in interacting polymer systems. The theoretical framework and numerical method of solving the self-consistent equations are presented. In this paper, different structures of polymer can be considered, such as homopolymer, block copolymer, polydisperse polymer and charged polymer. Several systems, micro/macro phase separation, interface, self-assembly, are presented as examples to demonstrate its applications in details. Besides, the fluctuation effects are considered. The first order is Gaussian fluctuation theory, which can be used to determine the stability of the mean-field solution and predict the kinetics of unstable structure. The derivation and applications of Gaussian fluctuation theory are presented as well.

Keywords self-consistent field theory (SCFT), Gaussian fluctuation theory, self-assembly, adsorption, depletion, polyelectrolyte, confinement

1 Introduction

Polymers, or macromolecules, are created by linking together small units, so-called "monomers", forming molecules with very high molecular weights. The simplest and the most typical polymers are linear chains formed from a single strand of monomers, while various architectures, such as bottlebrush, stars and rings, can also be obtained by the developments of the synthetic techniques. Furthermore, the monomers themselves also come in a rich variety, which can generate great effects on the monomer interactions and chain flexibility. In mesoscopic scale, the conformations of the polymer chains, which are sensitive to the external disturbance, such as temperature, and pH, play an important role on the properties of interface. These give polymers very different characteristics, which offer great potential for industrial applications and material designs. As a result, the study on polymers has flourished over the past decades and become one of the dominant fields in soft condensed matter sciences.

The present paper mainly focuses on the theoretical studies on the polymeric systems whose physics is dominated by the statistical mechanics of the conformational states of the polymers. This allows us to omit the atomic details and use a mesoscopic or coarse-grained model to depict the polymer chains, which not only gives the simplicity but also retains the physics nature [1]. However, even with this simplification, a polymeric system is still a complicated many-body system, which often requires intractable computational efforts. An effective strategy to deal with such system is the statistical field theory, in which one or more continuous fields are regarded as the fundamental degrees of freedom. One of the most successful field theories is the so-called self-consistent field theory (SCFT), which has been a powerful theoretical method to study the inhomogeneous polymer systems. The theoretical framework of SCFT is first used by Edwards and coworkers to study the single chain properties in melts and solutions [2], and then it has been expanded gradually to deal with many other topics in polymer sciences [3–7].

Within the framework of SCFT, due to the universality of polymers, the fundamental degrees of freedom of a polymer system can be effectively captured by several continuous field variables in a coarse-grained level. As in statistical mechanics, the main physical quantity needed to be calculated is the partition function or the free energy, which constitutes a functional integral of the continuous field variables. In general, this functional integral cannot be solved exactly due to the complexity of the Hamiltonian functional. As in most of the many-body theories, the first step along the theoretical development resorts to the mean-field approximation [2], which leads to the self-consistent mean-field theory (SCMFT) widely used in the theoretical polymer physics community. By SCMFT, the equilibrium structures of an inhomogeneous polymer system can be calculated in a mean-field level, providing a guide to experimentalists for finding structures in a particular system. Starting with the SCMFT, fluctuation effects, which always exist in a real system, can be taken into account order by order within the framework of a perturbation field theory [4–7]. Especially, the next step beyond the mean-field theory is the Gaussian fluctuation theory, by which the Hamiltonian functional of the system is expanded to the Gaussian level. The linear stabilities of different equilibrium structures (appeared as the solutions of a

Received August 31, 2011; accepted October 9, 2011
1. Department of Physics, Beijing Normal University, Beijing 100875, China
2. Institute of Chemistry, Chinese Academy of Sciences, Beijing 100190, China
E-mail: yandd@bnu.edu.cn

SCMFT) can be analyzed by Gaussian fluctuation theory and the spinodal lines of these structures can be calculated then. Around the critical point in the phase diagram of a polymer system, the fluctuations become so strong that they cannot be well described with Gaussian fluctuation theory, and the renormalized field theories, such as the self-consistent Hartree theory and the renormalization group theory, are needed.

Compared with molecular simulations, SCFT is a much better theoretical method to investigate the system with multicomponents or multiphases, because the thermodynamic limit of the system can be studied and then the phase boundary can be determined. Even the coexistent regions in such a complex system like diblock copolymers in selective solvents can be found [8]. Furthermore, while the polydispersity, which is intrinsic to polymer systems, is hard to be studied by molecular simulations, it can be well described with field theory. So far the SCFT is still the most efficient way to study or predict the properties of polymer systems, even the GPU has been used in molecular simulations nowadays. Although SCFT is in principle a statistical theory of the equilibrium states, many dynamic properties of a near-equilibrium system can also be investigated by combining SCFT with appropriate transport procedures, e.g., diffusion. In the present paper, we only focus on the applications to the equilibrium systems. The other applications incorporating fluctuations and dynamics in SCFT can be referred to the other literature [9].

This paper is organized as follows. First, we review the theoretical framework of SCMFT briefly. Several examples are given to demonstrate the power of SCMFT. Second, the Gaussian fluctuation theory is reviewed and its application is illustrated by studying the confinement effects on diblock copolymer melts.

2 Self-consistent mean-field theory (SCMFT)

To start, we consider some chain-like polymers, such as polyethylene and polyvinyl chloride. In reality, different polymers could have quite different chemical compositions. Considering their high molecular weights, one might expect it an intractable task to model the macromolecules. However, the problem is indeed simplified by the size of these huge molecules. On one hand, chain-like macromolecules, which include most commercial synthetic polymers, can always be considered to be flexible as long as the chemical bonds in the polymer backbone have the ability of relatively unhindered rotations. On the other hand, for a polymer, one can always find a length scale beyond which the chemical details of the molecule are no longer important. As a result, different polymers can be regarded as similar flexible coils, leading to universal properties among various polymer types. For example, the characteristic size of a high-molecular-weight in a homogeneous environment scales with the degree of polymerization to a universal exponent, while the chemical details of the monomer have effects only on the proportionality constant. In addition, the "flexibility" of a polymer chain also implies large numbers of available conformational states of the molecule, which results in a huge interdigitation among the polymers. Thus the fluctuations in the environment of each polymer chain could be very small, which in turn makes the mean-field technique become highly effective.

With these considerations, each polymer chain can be modeled as a simple mathematical space curve with the position vector of the s-th monomer of the i-th chain denoted as $\boldsymbol{r}_i^{\alpha}(s)$. (The subscript α will be used to label different monomers when we treat specific systems.) Then, we can define the volume fraction operator for the monomers

$$\hat{\phi}_{\alpha}(\boldsymbol{r}) = \rho_0^{-1}\sum_{i=1}^{n_{\alpha}}\int_0^{N_i} \mathrm{d}s\,\delta(\boldsymbol{r}-\boldsymbol{r}_i^{\alpha}(s)) \tag{1}$$

where ρ_0^{-1} is the volume of one monomer; N_i is the degree of polymerization of the i-th chain; n_{α} is the number of polymer chains of species α. The quantity measured by experiments is the ensemble average of this operator

$$\phi_{\alpha}(\boldsymbol{r}) \equiv \langle \hat{\phi}_{\alpha}(\boldsymbol{r}) \rangle \tag{2}$$

Here, the average is with respect to the conformational fluctuations of chains.

Obviously, certain partition function is required to evaluate this ensemble average. To begin with, denote the energy of the i-th chain of species α as $E[\boldsymbol{r}_i^{\alpha};0,N_i]$. (The square brackets are used hereafter to denote a functional.) Throughout this paper, we always assume that the polymer chains are flexible Gaussian coils and the environment exerts its influence on any chain through a mean field, w_{α}. Thus, the energy has the formula

$$\frac{E[\boldsymbol{r}_i^{\alpha};0,N_i]}{k_BT} = \int_0^{N_i}\mathrm{d}s\left(\frac{3}{2b_{\alpha}^2}\left|\frac{\partial \boldsymbol{r}_i^{\alpha}(s)}{\partial s}\right|^2 + w_{\alpha}(\boldsymbol{r}_i^{\alpha}(s))\right) \tag{3}$$

where b_{α} is the Kuhn length of species α. Then the single chain partition function can be written as

$$\mathcal{Q}_i^{\alpha}[w_{\alpha}] = \frac{1}{V}\int \mathcal{D}\boldsymbol{r}_i^{\alpha}\exp\left(-\frac{E[\boldsymbol{r}_i^{\alpha};0,N_i]}{k_{\mathrm{B}}T}\right) \tag{4}$$

This is a functional integral over all possible chain conformations, $\boldsymbol{r}_i^{\alpha}(s)$, for $0 < s < N_i$, weighted by the appropriate Boltzmann factor. To calculate this functional integral, let us consider the first s monomers of the chain with its two ends constrained. The partition function of this fragment is

$$Q_i^{\alpha}(\boldsymbol{r},\boldsymbol{r}_0,s)=\int\mathcal{D}\boldsymbol{r}_i^{\alpha}\exp\left(-\frac{E[\boldsymbol{r}_i^{\alpha};0,s]}{k_{\mathrm{B}}T}\right)\delta(\boldsymbol{r}_i^{\alpha}(0)-\boldsymbol{r}_0)\delta(\boldsymbol{r}_i^{\alpha}(s)-\boldsymbol{r}) \tag{5}$$

It can be proved that $Q_i^{\alpha}(\boldsymbol{r},\boldsymbol{r}_0,s)$ satisfies the modified diffusion equation (MDE)

$$\frac{\partial Q_i^{\alpha}(\boldsymbol{r},\boldsymbol{r}_0,s)}{\partial s}=\frac{b_{\alpha}^2}{6}\nabla^2 Q_i^{\alpha}(\boldsymbol{r},\boldsymbol{r}_0,s)-w_{\alpha}(\boldsymbol{r})Q_i^{\alpha}(\boldsymbol{r},\boldsymbol{r}_0,s) \tag{6}$$

with the initial condition, $Q_i^{\alpha}(\boldsymbol{r},\boldsymbol{r}_0,0)=\delta(\boldsymbol{r}-\boldsymbol{r}_0)$.

Similarly, the complementary partition function for the last N–s monomers is defined as

$$Q_i^{\alpha+}(\boldsymbol{r},\boldsymbol{r}_1,s)=\int\mathcal{D}\boldsymbol{r}_i^{\alpha}\exp\left(-\frac{E[\boldsymbol{r}_i^{\alpha};s,N_i]}{k_{\mathrm{B}}T}\right)\delta(\boldsymbol{r}_i^{\alpha}(N)-\boldsymbol{r}_1)\delta(\boldsymbol{r}_i^{\alpha}(s)-\boldsymbol{r}) \tag{7}$$

and satisfies the MDE

$$\frac{\partial Q_i^{\alpha+}(\boldsymbol{r},\boldsymbol{r}_1,s)}{\partial s}=-\frac{b_{\alpha}^2}{6}\nabla^2 Q_i^{\alpha+}(\boldsymbol{r},\boldsymbol{r}_1,s)+w_{\alpha}(\boldsymbol{r})Q_i^{\alpha+}(\boldsymbol{r},\boldsymbol{r}_1,s) \tag{8}$$

with the initial condition $Q_i^{\alpha+}(\boldsymbol{r},\boldsymbol{r}_1,N)=\delta(\boldsymbol{r}-\boldsymbol{r}_1)$.

To proceed, it is convenient to introduce two partial partition functions, which are defined by

$$q_i^{\alpha}(\boldsymbol{r},s)=\int\mathrm{d}\boldsymbol{r}_0 Q_i^{\alpha}(\boldsymbol{r},\boldsymbol{r}_0,s) \tag{9}$$

and

$$q_i^{\alpha+}(\boldsymbol{r},s)=\int\mathrm{d}\boldsymbol{r}_1 Q_i^{\alpha+}(\boldsymbol{r},\boldsymbol{r}_1,s) \tag{10}$$

These two functions also obey Eq. (6) and Eq. (8) with initial conditions, $q_i^{\alpha}(\boldsymbol{r},0)=1$ and $q_i^{\alpha+}(\boldsymbol{r},N)=1$, respectively. Obviously, the full partition function, $\mathcal{Q}[w]$, is related to the integral of the partial partition functions,

$$\mathcal{Q}_i^{\alpha}[w_{\alpha}]=\frac{1}{V}\int\mathrm{d}\boldsymbol{r}q_i^{\alpha}(\boldsymbol{r},s)q_i^{\alpha+}(\boldsymbol{r},s) \tag{11}$$

Within a mean-field picture, the ensemble-averaged volume fraction can be evaluated by

$$\phi_{\alpha}(\boldsymbol{r})=\rho_0^{-1}\sum_{i=1}^{n_{\alpha}}\frac{1}{\mathcal{Q}_i^{\alpha}[w_{\alpha}]V}\int\mathcal{D}\boldsymbol{r}_i^{\alpha}\int_0^{N_i}\mathrm{d}s\delta(\boldsymbol{r}-\boldsymbol{r}_i^{\alpha}(s))\exp\left(-\frac{E[\boldsymbol{r}_i^{\alpha};0,N_i]}{k_{\mathrm{B}}T}\right)$$

$$=\sum_{i=1}^{n_{\alpha}}\frac{1}{\rho_0\mathcal{Q}_i^{\alpha}[w_{\alpha}]V}\int_0^{N_i}\mathrm{d}sq_i^{\alpha}(\boldsymbol{r},s)q_i^{\alpha+}(\boldsymbol{r},s) \tag{12}$$

Furthermore, if the polymer chains of the same species are indistinguishable, such as the cases studied in this paper, the subscript i in above equations can be dropped and then Eq. (12) is simplified as

$$\phi_{\alpha}(\boldsymbol{r})=\frac{n_{\alpha}}{\rho_0\mathcal{Q}_{\alpha}[w_{\alpha}]V}\int_0^N\mathrm{d}sq_{\alpha}(\boldsymbol{r},s)q_{\alpha}^{+}(\boldsymbol{r},s)$$

$$=\frac{\overline{\phi}_{\alpha}}{\mathcal{Q}_{\alpha}[w_{\alpha}]N}\int_0^N\mathrm{d}sq_{\alpha}(\boldsymbol{r},s)q_{\alpha}^{+}(\boldsymbol{r},s) \tag{13}$$

where $\overline{\phi}_{\alpha}=n_{\alpha}N/\rho_0V$ is the average volume fraction of species α.

Obviously, evaluating the above quantities requires enough knowledge about the mean field w_{α}. Physically speaking, this field depends on the mutual interaction between segments and thus is coupled with the density profile. To determine this field self-consistently, it is necessary to have adequate information of the system and then give the partition function of the whole system, which always has the formula as follows:

$$Z=\int\left(\prod_{\alpha}\mathcal{D}\phi_{\alpha}\mathcal{D}w_{\alpha}\right)\exp\left(-\mathcal{F}[\{\phi_{\alpha}\},\{w_{\alpha}\}]\right) \tag{14}$$

The precise expression of the functional, $\mathcal{F}[\{\phi_{\alpha}\},\{w_{\alpha}\}]$, which is related to the physics details of the system, will be given for each example in the next section. It is noteworthy that, at the mean-field level, a self-consistent condition should be satisfied, i.e.,

$$\frac{\delta\mathcal{F}[\{\phi_{\alpha}\},\{w_{\alpha}\}]}{\delta\phi_{\alpha}(\boldsymbol{r})}=0 \tag{15}$$

This equation, together with Eq. (13) and other necessary conditions (e.g. the condition of incompressibility), comprises a set of self-consistent equations, from which the field w_{α} and the properties of the system can be obtained.

The SCMFT equations are a set of highly nonlinear equations, especially, the MDEs is non-local partial differential equations. Generally, there is no exact analytical solution except the trivial homogeneous case, so people usually resort to the numerical methods. We will not show details of the numerical methods here. Instead, we only give a brief review. One can solve the MDE both in real space and reciprocal space. In real space, the finite difference algorithm is used for the Laplace operator and to update the propagator along s direction with certain appropriate strategies, such as Crank-Nicolson method for one-dimensional system and the alternating direction implicit (ADI) method for high dimensional systems. This method is easy to achieve, especially for the system with complex boundary, such as the polymers interact with chemical patented surface, or stay between two spherical particles [10]. Alternatively, for the system with known periodic structure, it is better to perform the computation in a reciprocal space with high accuracy which is called the spectral method [6]. Since it is hard to include defects which

involve a lot of modes, this is a most powerful tools to investigate the self-assembly of block copolymer in bulk phase. Actually, the first three-dimensional SCFT calculation was performed in a reciprocal space [11]. The auxiliary field is local in real space while the Laplace operator is local in the reciprocal space, so both these two methods have to face the non-local problem. A new efficient way to deal with this is the pseudo spectral method. By splitting the evolution operator, the update of the diffuse equation becomes

$$q(\boldsymbol{r},s+\Delta s) \approx \exp\left(-\frac{1}{2}\Delta s\omega(\boldsymbol{r})\right)\exp\left(\Delta s\nabla^2\right)\left(-\frac{1}{2}\Delta s\omega(\boldsymbol{r})\right)q(\boldsymbol{r},s) \tag{16}$$

In pseudo spectral method, the propagator is transformed into a reciprocal space before the operator $\exp(\Delta s\nabla^2)$ acts on it, and then is transformed back into the real space before the operator $\exp[-\Delta s\omega(\boldsymbol{r})/2]$ acts on it,

$$q(\boldsymbol{r},s+\Delta s) \approx \exp\left(-\frac{1}{2}\Delta s\omega(\boldsymbol{r})\right)\ F^{-1} \left\{\exp\left(\Delta s\nabla^2\right)\ F\left[\exp\left(-\frac{1}{2}\Delta s\omega(\boldsymbol{r})\right)q(\boldsymbol{r},s)\right]\right\} \tag{17}$$

where F is the Fourier transformation and F^{-1} is the inverse Fourier transformation. Thus, both the auxiliary field operator and the Laplace operator are local. By virtue of the fast Fourier transformation algorithm, the MDE can be solved with high accuracy and efficiency. Since the non-local MDE become local in this method, the SCFT computation can be performed in parallel with MPI or on a GPU [12].

There are several methods to converge the SCFT equations. Simple mixing is the simplest one. This is an explicit method usually costing long time due to its bad stability. Broyden method, which is an implicit one, is a more stable and accurate method. Although it needs only to inverse the Jacobian for the first step, it still needs demanding computation. Therefore, it is commonly used only for the one-dimensional problem. Even for a two-dimensional system, it is too expensive. By expanding the chemical potential in implicit algorithm around the field of old step, a semi-implicit method can be obtained. If the Jacobian (expanding coefficient) is approximated by that in homogeneous system, which is always diagnosed, this method provides very efficient performance and is easy to be applied to the high dimensional system [13]. But now it is used merely on one or two components system. For many-component systems it still needs improvement. So far the most convincing and reliable method is Anderson mixing, which mixes several past steps to maintain the history and improve the stability, and it shows very good performance both in real [14] and reciprocal space [15] in any dimensional and multi-components systems.

3 Applications of SCMFT in several polymeric systems

3.1 Mixtures of polymers and colloid particles [10,16–17]

Mixtures of polymers and colloid suspensions are widely used in many industrial applications, including adhesion and lubrication. In many cases polymers can interact strongly with the colloidal particles. In this system, there are two effects. One is the adsorption effect for the adsorbing polymers, which is induced by the attractive interaction between the monomer and the surface [16]; the other is the depletion effect for the non-adsorbing polymer, which leads to the polymer concentration near the surface lower than that in the bulk [10]. The adsorption effect and the depletion effect always coexist in the mixture of polymers and colloidal particles. However, the former is the main effect for a system containing small amounts of colloidal particles, while the latter will become important when the concentration of the colloidal particles is high enough to make the colloidal particles much closer. These two limit cases, in which the two effects can be treated separately, will be presented in this subsection.

Consider a polymer solution containing colloid particles that are modeled as spherical objects with radius R [16]. The particle surface is impenetrable and the adsorption is reversible. The indices p and s below are used to label the polymer and solvent molecules, respectively. Within SCMFT, the free energy of the system is given by

$$\frac{F}{\rho_0} = \chi\int \mathrm{d}\boldsymbol{r}\phi_{\mathrm{p}}(\boldsymbol{r})\phi_{\mathrm{s}}(\boldsymbol{r}) - \sum_{\alpha=\mathrm{p,s}}\int \mathrm{d}\boldsymbol{r}\phi_\alpha(\boldsymbol{r})w_\alpha(\boldsymbol{r}) + \int \mathrm{d}\boldsymbol{r}U(\boldsymbol{r})\phi_{\mathrm{p}}(\boldsymbol{r}) - \frac{\overline{\phi}_{\mathrm{p}}V}{N}\ln\mathcal{Q}_{\mathrm{p}} - \overline{\phi}_{\mathrm{s}}V\ln\mathcal{Q}_{\mathrm{s}} \tag{18}$$

and the SCMFT equations are given by

$$\phi_{\mathrm{p}}(\boldsymbol{r}) = \frac{\overline{\phi}_{\mathrm{p}}}{\mathcal{Q}_{\mathrm{p}}N}\int_0^N \mathrm{d}sq(\boldsymbol{r},s)q(\boldsymbol{r},N-s) \tag{19}$$

$$\phi_{\mathrm{s}}(\boldsymbol{r}) = \frac{\overline{\phi}_{\mathrm{s}}}{\mathcal{Q}_{\mathrm{s}}}e^{-w_{\mathrm{s}}(\boldsymbol{r})} \tag{20}$$

$$w_{\mathrm{p}}(\boldsymbol{r}) = \chi\phi_{\mathrm{s}}(\boldsymbol{r}) + U(\boldsymbol{r}) + \eta(\boldsymbol{r}) \tag{21}$$

$$w_{\mathrm{s}}(\boldsymbol{r}) = \chi\phi_{\mathrm{p}}(\boldsymbol{r}) + \eta(\boldsymbol{r}) \tag{22}$$

$$\phi_{\mathrm{p}}(\boldsymbol{r}) + \phi_{\mathrm{s}}(\boldsymbol{r}) = 1 \tag{23}$$

This set of equations is solved by the real-space method. The

conventional procedure is as follows. First, some initial values are given to $w_p(\boldsymbol{r})$ and $w_s(\boldsymbol{r})$ at each grid point. Second, the MDE, Eq. (6) is solved using the Crank-Nicholson method. Then the convergence results are obtained by a simple mixing method.

Let us consider the case in which the colloidal particles are so far from each other that the system can be treated as a spherically symmetric one with the colloidal particle at the center. The polymers interact with the colloidal particle by the effective adsorbing potential, $U(\boldsymbol{r})$, that is assumed to be a rectangular-form potential for simplicity, i.e.,

$$U(\boldsymbol{r}) = \begin{cases} 0, & r > R + d \\ -U_0, & R \leqslant r \leqslant R + d \end{cases} \tag{24}$$

where r is the radial distance from the center of the colloidal particle and d is the force range of the potential.

The conformation of the adsorbed polymers can be described in terms of loops and tails, since the train part is not important for small particles. To calculate these structures, we need to define the adsorbed layer as follows. At the surface of the colloidal particle, the polymer density is zero because of the impenetrability of the surface. Between the surface of the colloidal particle and the infinite distance the density profile has one maximum and two inflections. The distance from the origin to the second inflection, which is between the infinite distance and the sphere where the density profile has the maximum, is denoted by r_w. The region between the surface of the colloidal particle and the sphere corresponding to the location of r_w is called the boundary layer. The region outside the boundary layer is defined as the adsorbed layer, where the polymer density is higher than that in bulk solution. We divide the adsorbed layer into two parts, the adsorbed part and the free part. A polymer will be an adsorbed polymer if any part of it falls into the boundary layer, while the free polymers are those with none of their monomers in the boundary layer. The total propagator $q(\boldsymbol{r}, s)$ can be divided into the adsorbed and free ones, i.e., $q(\boldsymbol{r}, s) = q^a(\boldsymbol{r}, s) + q^f(\boldsymbol{r}, s)$. The propagator of adsorbed chain $q^a(\boldsymbol{r}, s)$ and the propagator of free chain $q^f(\boldsymbol{r}, s)$ satisfy the same MDE as $q(\boldsymbol{r}, s)$, but with different boundary conditions. The propagator of free chain vanishes at the adsorbed layer wall, i.e., $q^f(\boldsymbol{r},s)\big|_{r=r_w} = 0$, and $q^a(\boldsymbol{r}, s)$ can be obtained from $q^f(\boldsymbol{r}, s)$. Using the propagators of the adsorbed chain and free chains we can split the total volume fraction into three parts, i.e., loop, tail and free parts. The volume fraction of segments coming from loops, tails and free chains are given by

$$\phi_p^l(\boldsymbol{r}) = \frac{\overline{\phi}_p}{\mathcal{Q}_p N} \int_0^N \mathrm{d}s q^a(\boldsymbol{r},s) q^a(\boldsymbol{r},N-s) \tag{25}$$

$$\phi_p^t(\boldsymbol{r}) = \frac{2\overline{\phi}_p}{\mathcal{Q}_p N} \int_0^N \mathrm{d}s q^a(\boldsymbol{r},s) q^f(\boldsymbol{r},N-s) \tag{26}$$

$$\phi_p^f(\boldsymbol{r}) = \frac{\overline{\phi}_p}{\mathcal{Q}_p N} \int_0^N \mathrm{d}s q^f(\boldsymbol{r},s) q^f(\boldsymbol{r},N-s) \tag{27}$$

The average tail length, l_{tail}, and the average loop length, l_{loop}, can be obtained by

$$l_{tail} = \lim_{r \to r_w^+} \frac{\int_0^N s q^a(r,N-s) q^f(r,s) \mathrm{d}s}{\int_0^N q^a(r,N-s) q^f(r,s) \mathrm{d}s} \tag{28}$$

$$l_{loop} = \lim_{\substack{r_1 \to r_w^+ \\ r_2 \to r_w^+}} \frac{\iint q^a(r_1,s_1) Q^f(r_1,r_2,s) q^a(r_2,N-s-s_1) s \mathrm{d}s_1 \mathrm{d}s}{\iint q^a(r_1,s_1) Q^f(r_1,r_2,s) q^a(r_2,N-s-s_1) \mathrm{d}s_1 \mathrm{d}s} \tag{29}$$

In the numerical calculations the potential width d is taken as twice the Kuhn length, i.e., $d = 2b$, while the adsorption potential is $U_0 = -0.4$. In general, chain configurations in the proximity of surface are affected significantly by the nature of polymer-surface interaction. In particular, the change of average tail length with curvature is nearly independent of the material nature of polymer-surface interaction as long as the interaction is strong enough.

Figure 1 shows the decomposition of the polymers density profiles into tail, loop and free parts. One can find that the tails are the dominant part at some distance away from the surface, while in the inner region of the absorbed layer near the surface, loops are the dominant part.

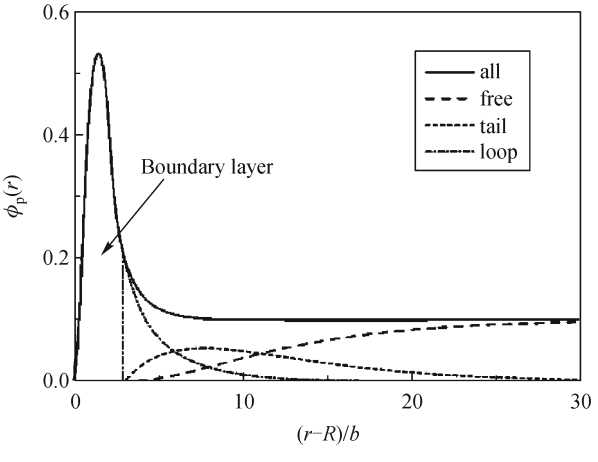

Figure 1 Polymer segments distributions belong to tail, loop, and free part. The parameters are taken as $N = 1000$, $\phi_p^0 = 0.1$, $\chi = 0.4$ and $R/b = 10$.

Figure 2 presents the most important results of this study. It demonstrates how the average tail length, l_{tail}, changes with the normalized particle radius, R/R_g, for different bulk concentrations. One can find that l_{tail} increase with the decreasing particle radius, which is distinct, especially, when R is smaller than R_g. When R decreases, the dangling tails have less possibility to come back onto the surface with the other end, and hence the tails can be longer. When the bulk concentration of polymer increases, the curvature effect becomes weak because of the excluded volume effect of polymer.

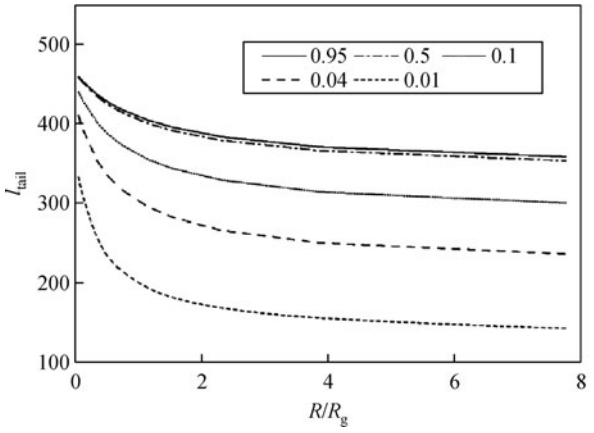

Figure 2 Average tail length, l_{tail}, as a function of normalized particle radius, R/R_g, at different bulk concentrations of $\phi_p^0 = 0.01$, 0.04, 0.1, 0.5, and 0.95, respectively. $N = 1000$; $\chi = 0.2$.

Up to now, the analysis is restricted to the system containing one colloidal particle, which is a good approximation for the case of low colloid concentration. Contrarily, for the non-adsorbing system, if the concentration of the colloidal particle is high, the particles can be quite close to each other and then the depletion effect becomes important. As a first glance to the depletion effect, let us consider a polymer solution containing two equal-size spherical particles, the separation between which is h (the shortest distance between any two points of the two particles). To focus on the effect of the depletion, we switch off the adsorption effect by taking U_0 as zero in this case. The procedure of solving the SCMFT equations is almost the same as that mentioned above. However, for the system containing two particles, the spherical symmetry no longer exists and it is convenient to use bi-spherical coordinate [10]. Because the system is axisymmetrical about the axis connecting the centers of the two spherical particles, the calculation is of two-dimension rather than three-dimension. In this case, the MDE is solved by the ADI method.

In addition to the quantities mentioned before, two extra quantities are defined to characterize the depletion effect. One is the depletion potential, $U(h)$, between the two spheres,

$$U(h) = F(h) - F(\infty)$$

The other is the depletion amount, $\Gamma(\infty)$–$\Gamma(h)$, where

$$\Gamma(h) = \int_V \mathrm{d}\boldsymbol{r}\left(\phi_p(\boldsymbol{r}) - \overline{\phi}_p\right)$$

Figure 3 shows the depletion potential, $U(h)$, (a and b) and the depleted amount, $\Gamma(\infty) - \Gamma(h)$, (c and d) as a function of the separation h, in dilute regime (a and c) and semidilute regime (b and d). In the dilute case, the polymer chains can be regarded as isolated coils. The trends of the depletion potential are similar to those between two plates, in which the depth increases with increasing polymer concentrations. The range of potential remains nearly constant, which is about the order of the natural polymer size.

In the semidilute case, the coils begin to overlap and the range of the potential decreases with the increase of polymer concentration. Since the depletion potential comes from the overlap of two depletion layers belonging to two spheres, and the thickness of depletion layer decreases with increasing polymer concentration, the depletion potential has the same width as the thickness of depletion layer. Different from dilute case, the minus of depleted amount, $\Gamma(\infty) - \Gamma(h)$, exhibits a barrier in the present case. This indicates that when the two spheres approach to each other, the depletion layers belong to the two spheres begin to overlap, and the total number of polymers in between first decreases to the minimum, and then goes up. The height of barrier increases with increasing polymer concentration. On the other hand, in dilute case, the total number of polymers in between always increases with decreasing h. This discrepancy indicates qualitatively different depletion effects in dilute regime and semidilute regime. Anyway, in both cases the depletion interaction is always attractive. Since there is no enthalpic attractive effect in these calculations, this attraction has a totally entropic origin.

In addition to the cases considered above, two other important factors always exist in a real system. One is the polydispersity of the polymers. Because of the conformational entropy, shorter polymer chains can stay in between than the longer chains. In other words, shorter polymer chain has stronger depletion effect than the longer chain. It can be concluded by the SCMFT calculation that the polydispersity increases the range of the depletion potential, while it decreases the depth of the potential [17]. The other point is the coupling of adsorption and depletion. It can be imagined that if an adsorbing potential is present, the polymers will be harder to be excluded from the gap between adjacent particles. As a result, an effective repulsive force can emerge and there will be an energy barrier on the potential profile of the two particles. This effect has been verified for the plate case, and the case of two spherical particles has been studied.

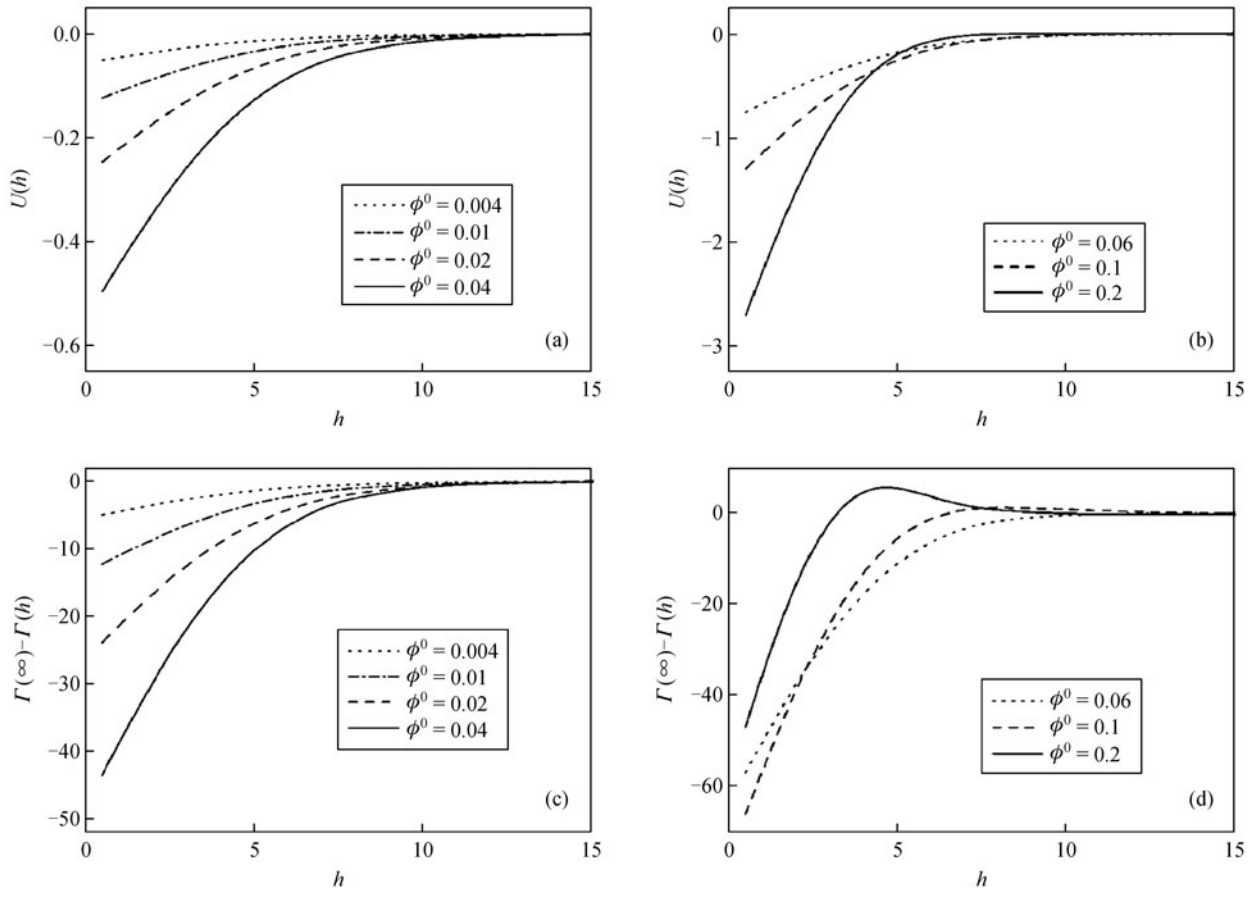

Figure 3 The depletion potential (a, b) and depleted amount (c, d) between two spheres as a function of the separation h in dilute (a, c) and semidilute (b, d) solutions. The parameters are taken as $\chi = 0.5$, $N = 100$, and $R/b = 10$.

3.2 Weakly charged polyelectrolytes in charged cylindrical systems [18,19]

As is well known, polyelectrolytes (PEs) form an important class of polymeric materials. Specially, most of bio-macromolecules are PEs, for example DNA, RNA, et al. These macromolecules contain chemical groups which are capable of dissociation in polar solvents, producing charged species. As a result, the Coulombic interaction, which is known as a famous long-ranged interaction, plays an important role as well as other short-ranged interactions in the system. This peculiarity not only brings novel properties and phase behaviors, but also gives great complexities and challenge to theoretical studies.

In this subsection, we restrict the attention to the simplest case of a linear weakly charged homo-polyelectrolytes dissolved in a polar solvent. The words "weakly charged" means the case in which the charge quantity of each chain is so small that the chain can still be treated as a random coil. It is assumed that each polyelectrolyte chain is negatively charged and the charge is smeared along the chain with a charge fraction p. Besides n_p polyelectrolyte chains, there are also n_s neutral solvent molecules, n_+ canions and n_- anions in a finite volume V. Integral variables v_p, v_+ and v_- are the valence numbers of polyelectrolyte monomers, canions and anions, respectively. The volumes of the small ions are ignored. By SCMFT, the free energy functional of the system is given by

$$\frac{F}{\rho_0} = \int \mathrm{d}\boldsymbol{r}(\chi_{ps}\phi_p(\boldsymbol{r})\phi_s(\boldsymbol{r}) - ew_e(\boldsymbol{r})\phi_e(\boldsymbol{r})) + \sum_{j=p,s,+,-}\int \mathrm{d}\boldsymbol{r}(\mu_j\phi_j(\boldsymbol{r}) - w_j(\boldsymbol{r})\phi_j(\boldsymbol{r})) + \int \mathrm{d}\boldsymbol{r}U(\boldsymbol{r})\phi_p(\boldsymbol{r}) + \int \mathrm{d}\boldsymbol{r}\left(\phi_e(\boldsymbol{r})\varphi(\boldsymbol{r}) - \frac{b^2}{2\tau}|\nabla\varphi(\boldsymbol{r})|^2\right) - \sum_{j=p,s,+,-}\frac{\overline{\phi}_j V}{N_j}\ln\left(\frac{Q_j}{\overline{\phi}_j}\right) \quad (30)$$

where e is the unit charge; $\phi_e(\boldsymbol{r}) = -p\phi_p(\boldsymbol{r}) + \phi_+(\boldsymbol{r}) - \phi_-(\boldsymbol{r})$ is the charge density; $w_e(\boldsymbol{r})$ is the auxiliary field conjugated to the

charge density; $\varphi(\boldsymbol{r})$ is the electrostatic potential normalized by k_BT/e; μ_j and χ_{ps} are defined in Ref. 18, and $\tau = 4\pi\rho_0 b^2e^2/\varepsilon k_BT$, where ε is the dielectric constant, which is approximately a constant in the whole space. Hereafter, we only consider the monovalent system, i.e., $v_p = v_- = v_+ = -1$. $U(\boldsymbol{r})$ is the short-range non-Coulombic interaction between surface and polyelectrolytes, which has been given by Eq. (24).

With the presence of the electrostatic potential, $w_p(\boldsymbol{r})$ in the MDE of Eq. (6) is replaced by $w_p(\boldsymbol{r}) + p\varphi(\boldsymbol{r})$. Moreover, several additional equations are added to the set of the SCMFT equations. One is the Poisson-Boltzmann equation obeyed by $\varphi(\boldsymbol{r})$,

$$\nabla^2\varphi(\boldsymbol{r}) = -\tau\left\{-\nu_p p\phi_p(\boldsymbol{r}) + \frac{\nu_+\overline{\phi}_+}{\mathcal{Q}_+}\exp[-\nu_+\varphi(\boldsymbol{r})] - \frac{\nu_-\overline{\phi}_-}{\mathcal{Q}_-}\exp[-\nu_-\varphi(\boldsymbol{r})]\right\} \quad (31)$$

where

$$\mathcal{Q}_\pm = \frac{1}{V}\int d\boldsymbol{r}\exp[-\nu_\pm\varphi(\boldsymbol{r})]$$

The other is the charge neutrality constraint,

$$\nu_p p\overline{\phi}_p + \nu_+\overline{\phi}_+ + \nu_-\overline{\phi}_- + \frac{2r_0 b}{L^2}\sigma = 0 \quad (32)$$

where σ is the dimensionless reduced area density of the surface charge given by $\sigma \equiv \sigma_0/b^{-2}$, in which σ_0 is the area density of surface charge.

In addition, the volume fraction of the ions is given by

$$\phi_\pm(\boldsymbol{r}) = \frac{\overline{\phi}_\pm}{\mathcal{Q}_\pm}\exp[-\nu_\pm\varphi(\boldsymbol{r})] \quad (33)$$

As it is assumed that the anions totally come from the completely ionized salt molecules, the bulk concentration of the salt, $C_{s,b}$, is given by

$$C_{s,b} = \frac{\overline{\phi}_-}{\mathcal{Q}_-}\exp[-\nu_-\varphi(\infty)] = \frac{\overline{\phi}_-}{\mathcal{Q}_-}$$

where the infinite distance is defined as the zero point of the electrostatic potential. The bulk molar concentration is related to $C_{s,b}$ by the Avogadro's number N_A, i.e. $C^M_{salt} = C_{s,b}\rho_0/N_A$.

It is obvious that, for a system containing polyelectrolytes, the SCMFT equations are more difficult to be solved because of the presence of the two differential equations. A combination of the Broyden's method and a globally convergent strategy is used to solve the set of nonlinear equations. The MDE is discretized by using the Crank-Nicolson scheme.

Now we particularly focus on the problem of the adsorption of polyelectrolytes onto an oppositely charged cylinder with a radius r_0 and an area density of surface charge σ_0. This is motivated by the fact that, in biological systems, many charged objects have rod-like appearance, such as the tobacco mosaic virus, and the adsorption of polyelectrolytes onto these objects plays important roles in many processes of biological systems. Two interesting aspects will be covered in the follows. One is the adsorption-depletion transition, which is originated from the competition between the electrostatic attraction and the entropic repulsion. When polymer chains are adsorbed onto the surfaces, they will lose entropy. If the adsorption energy is not large enough to compensate the entropy loss, the PEs will not be adsorbed onto the surface, giving way to the adsorption-depletion transition. The other one is the charge inversion phenomenon. If the adsorption energy is large enough, one of the chain ends will be adsorbed strongly onto the surface. Because of the chain connectivity, the rest of the chain (with the opposite charges) is pulled near the surface, and results in an overcompensation of the origin surface charges by the adsorbed polyelectrolytes. Therefore, the surface-polyelectrolyte complex has a net opposite charges compared to the bare charged surfaces. The main quantities are the surface excess, Γ, and the charge inversion ratio, σ_{cp}/σ. Γ is defined as

$$\Gamma = \lim_{l\to\infty}\frac{1}{2\pi l}\int_V d\boldsymbol{r}(\phi_p(\boldsymbol{r}) - \phi_{p,b})$$

where l is the length along the charged cylinder; $\phi_{p,b}$ is the bulk concentration of the polyelectrolytes. Obviously, polymers are adsorbed by the surface when $\Gamma > 0$ and depleted from the surface when $\Gamma < 0$. The place where $\Gamma = 0$ corresponds to the adsorption-depletion transition.

The charge inversion ratio is given by

$$\sigma_{cp}/\sigma = 1 - p\Gamma/\sigma r_0$$

Charge inversion only happens when $\sigma_{cp}/\sigma < 0$, and the full charge inversion will be observed when $\sigma_{cp}/\sigma \leqslant -1$ for large non-Coulombic interaction U_0. On the other hand, $\sigma_{cp}/\sigma > 0$ means that no charge inversion happens.

Let us first present some numerical results about the adsorption-depletion transition. In this case we take $U_0 = 0$ to make the physics clearer. It has been demonstrated experimentally that at the adsorption-depletion transition point a scaling expression exists between the charge fraction of polyelectrolyte chains, p, the density of surface charge on the cylinder, σ, and the salt concentration, C^*_{salt}, for many systems of polyelectrolytes and oppositely charged micelles or dendrimers, i.e.,

$$C^*_{salt} \sim p^{\alpha(r_0)}\sigma^{\beta(r_0)}$$

We obtained the same scaling expression for different radius of the cylinder, r_0, which we do not present here to save space.

Fig. 4 shows the dependence of α and β on the surface curvature as well as the dependence of the critical salt concentration, C^*_{salt}, on the surface curvature. The surface curvature is changed by increasing the reduced cylinder radius, r_0/b, from 0.5 to 100. The results show that both α and β decrease as r_0 increases, while C^*_{salt} increases as r_0 increases. However, when the r_0 goes larger than $2R_g$, α, β, and hence C^*_{salt} nearly do not change with the r_0 and quickly converge to the values of the planar case. We define the point $r_0 \sim 2R_g$ as the crossover point, which divides the curvature dimension into two regimes, or, cylindrical regime for $r_0 < 2R_g$ and planar regime for $r_0 > 2R_g$. It is worth remembering that this crossover point is universal in the cylindrical system, because it is independent of other parameters. There are two reasons for the existence of the two different regimes in this system. One reason is that the polyelectrolyte chains have larger entropy loss when they are adsorbed on the surface with larger curvature (small r_0). The other reason is that the electrostatic field distribution along the radial direction is different at different r_0 for a given σ. These differences become small when r_0 increases comparable to the size of polyelectrolyte chain.

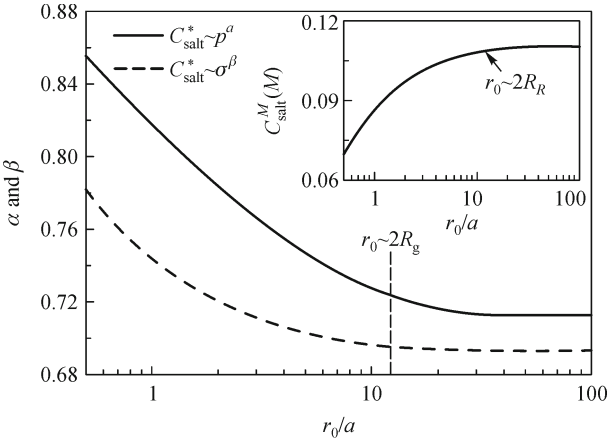

Figure 4 Effect of surface curvature on the scaling law. α and β are obtained for fixed $\sigma = 0.025$ and $p = 0.1$, respectively. α and β decrease as r_0 increases when $r_0 < 2R_g$. As r_0 goes larger than $2R_g$, α and β nearly do not change with r_0 and approach the fixed values of the planar surface, i.e., 2/3. The insert is the r_0 dependence of C^*_{salt}. C^*_{salt} increases as r_0 increases and quickly converges to the result of the planar surface as r_0 goes larger than $2R_g$. (a is used as the Kuhn length here instead of b.)

It is shown that if all the parameters are fixed except r_0, which can be easily done in experiments, the adsorption-depletion transition at a critical radius $r_{0,c}$ will happen. Figure 5 shows the critical $r_{0,c}$ as a function of C^M_{salt}. The left side corresponds to the adsorption regime while the right side corresponds to the depletion regime. The critical line in the cylindrical system is quite similar to that in a single chain

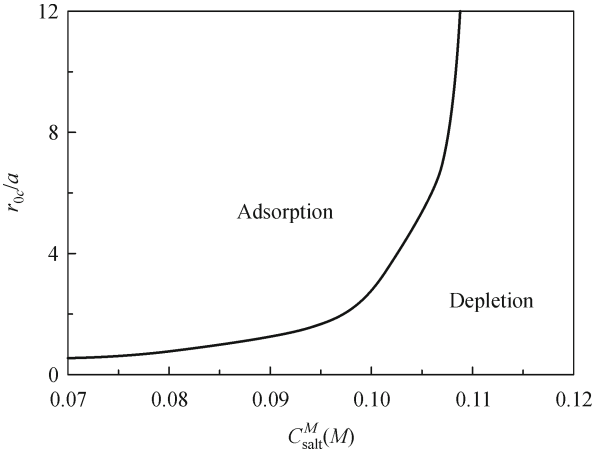

Figure 5 The C^M_{salt} dependence of the reduced critical radius, r_{0c}/a. (a is the Kuhn length here.) The critical line separates the adsorption regime from the depletion regime for $\sigma = 0.025$ and $p = 0.1$.

adsorption onto an oppositely charged spherical system, as reported in the references.

Now, we begin to investigate the charge inversion phenomenon with the presence of the short-range non-Coulombic interaction, $U(\boldsymbol{r})$. It can be imagined that, when $U(\boldsymbol{r})$ is weak, the adsorption process is dominated by the Coulombic interaction. This case is called the Coulombic interaction dominated regime, while the contrary case, in which the Coulombic interaction is relatively weak, is called the short-range non-Coulombic interaction dominated regime. These two regimes can be determined by varying U_0. By taking $U_0 = 0$ in salt-free solution, we can obtain the Coulombic interaction dominated regime. On the other hand, the short-range non-Coulombic interaction dominated regime should be determined by investigating the effect of salt concentration on the surface excess and charge inversion ratio for different values of U_0. The effects of surface excess, Γ, and charge inversion ratio, σ_{cp}/σ, on the salt concentration, $C_{s,b}$, have been studied in Ref. [19], in which we find that when the short-range non-Coulombic interaction becomes strong enough to dominate the polyelectrolyte adsorption process, both Γ and σ_{cp}/σ will increase in absolute values as $C_{s,b}$; otherwise, they both decrease with the increasing salt concentration.

Figures 6 and 7 show the effects of surface curvature, characterized by cylinder radius, r_0, on the charge inversion ratio σ_{cp}/σ. Figure 6 corresponds to the Coulombic interaction dominated regime ($U_0 = 0$), in which with decreasing the cylinder radius from $r_0 = 100$ to $r_0 = 12 \approx 2R_g$, σ_{cp}/σ decreases quite slowly. When the cylinder radius is less than $2R_g$, however, σ_{cp}/σ increases quickly, and no charge inversion happens in the large surface curvature regime

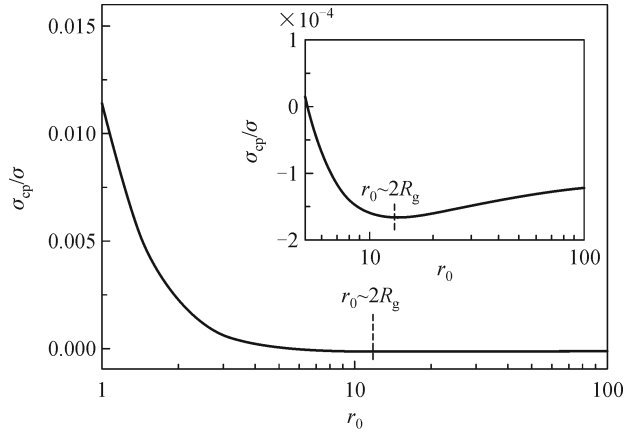

Figure 6 Cylindrical radius, r_0 (in unit of Kuhn length, b), dependence of the charge inversion ratio, σ_{cp}/σ, in the Coulombic interaction dominated regime with $C_{s,b} = 0$, $\sigma = 0.1$, $p = 0.5$, $\chi_{ps} = 0.1$ and $U_0 = 0$. The insert is the detail for the crossover point of r_0. Only moderate charge inversion ($\sigma_{cp}/\sigma \approx -2\times10^{-4}$) happens in this case.

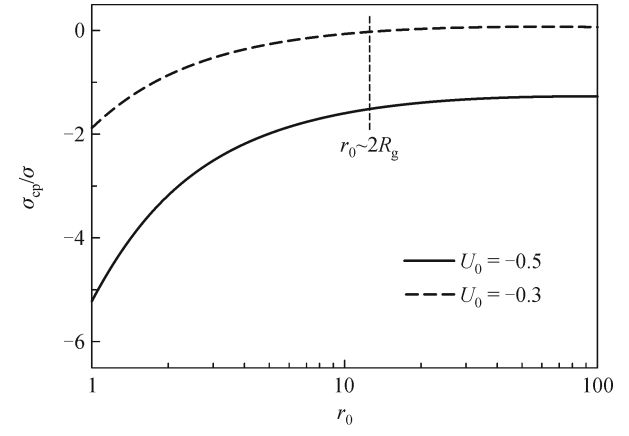

Figure 7 Charge inversion ratio, σ_{cp}/σ, as a function of cylindrical radius, r_0, (in unit of Kuhn length a) with $C_{s,b} = 0.1$, $\sigma = 0.025$, $p = 0.1$, and $\chi_{ps} = 0.1$ for different short-range non-Coulombic interactions, U_0. When $r_0 < 2R_g$, the magnitude of σ_{cp}/σ increases with decreasing r_0, and strong charge inversion $\sigma_{cp}/\sigma = -1.9$ and -5.2 have been obtained in large surface curvature (r_0= 1) for $U_0 = -0.3$ and -0.5, respectively. When $r_0 > 2R_g$, σ_{cp}/σ nearly does change with r_0.

(small r_0). Moreover, we can only observe a moderate charge inversion ($\sigma_{cp}/\sigma \approx -2\times10^{-4}$) at $r_0 \sim 2R_g$.

However, for both the short-range non-Coulombic interaction dominated regime ($U_0 = -0.5$) and the crossover regime ($U_0 = -0.3$), a different dependence of σ_{cp}/σ on r_0 has been found, as shown in Fig. 7, in which the magnitude of σ_{cp}/σ increases with decreasing r_0 at a high salt concentration ($C_{s,b} = 0.1$). Particularly, large charge inversion ratio $\sigma_{cp}/\sigma \approx -5.2$ has been observed in the large surface curvature limit ($r_0 = 1$) for $U_0 = -0.5$, that indicates that surface curvature does have strong effects on the PE charge inversion phenomena. Also, we can define, approximately, the point of $r_0 \sim 2R_g$ as a crossover point in these two figures. Besides, there is another important length scale which is the Debye screening length. When Debye length becomes comparable to the length of r_0, or $r_0 + d$, both these lengths will define the region where the curvature effects onto PE adsorption are important. Obviously, the crossover point of $r_0 \sim 2R_g$ is only reasonable in the systems with short-range non-Coulombic interaction and high salt concentration.

3.3 Nucleation in binary polymer blends [20]

It is well known that an initially homogeneous polymer blends can transform to an inhomogeneous one through changing the thermodynamic parameters (e.g., the temperature), which is always referred to as the phase separation. We also know that a phase separation process is not instantaneous and often involve the formation of microstructures that are the "nuclei" of the new phase which appears during the transformation. Note that the appearance of the nucleus of a new phase in effect implies the creation of an interface, which gives an increase to the free energy of the system. As a result, the nucleation phenomenon is an activated process, in which only the nuclei with enough size can grow to a new bulk phase[21].

Now we consider an incompressible blends of type A and type B linear, flexible homopolymers, in which species A can have polydisperse chain lengths. These two types of chains are modeled as Gaussian chains with degrees of polymerization N (the subscript A is omitted in case there is any confusion) and N_B, and the corresponding numbers of chains n_{AN} and n_B, respectively. For simplicity, both A and B monomers are assumed to have the same monomeric volume ρ_0^{-1} and Kuhn length b. The SCMFT equations are now

$$w_A(\boldsymbol{r}) = \chi\phi_B(\boldsymbol{r}) + \eta(\boldsymbol{r}) \tag{34}$$

$$w_B(\boldsymbol{r}) = \chi\phi_A(\boldsymbol{r}) + \eta(\boldsymbol{r}) \tag{35}$$

$$\phi_A(\boldsymbol{r}) = \frac{\phi_A^0}{N_0}\int_0^\infty \mathrm{d}N f_A(N) e^{w_A^0 N}\int_0^N \mathrm{d}s q_A(\boldsymbol{r},N-s) q_A(\boldsymbol{r},s) \tag{36}$$

$$\phi_B(\boldsymbol{r}) = \frac{1}{N_B}\int_0^{N_B} \mathrm{d}s q_B(\boldsymbol{r},N-s) q_B(\boldsymbol{r},s) \tag{37}$$

$$\phi_A(\boldsymbol{r}) + \phi_B(\boldsymbol{r}) = 1 \tag{38}$$

where ϕ_A^0 and w_A^0 are the average volume fraction and the auxiliary filed in the bulk, respectively, for A chains. $f_A(N)$ is the chain length distribution function, which is adopted by the continuous Schulz distribution for reflecting realistic chain length distribution given by

$$f_{\mathrm{A}}(N)=\frac{N^{k-1}k^k}{N_0^k\Gamma(k)}\exp(-kN/N_0) \tag{39}$$

where N_0 is the number-average chain length, and k is a parameter related to the polydispersity index. Smaller k corresponds to more polydisperse distribution, and infinite k corresponds to a monodisperse case.

The properties of a nucleus can be described by the volume fraction, $\phi_{\mathrm{A}}(\boldsymbol{r})$, and materials excess, $\tilde{M}^{\mathrm{ex}}$, which is defined as

$$\tilde{M}^{\mathrm{ex}}=\frac{1}{N^{3/2}b^3}\int \mathrm{d}\boldsymbol{r}(\phi_{\mathrm{A}}(\boldsymbol{r})-\phi_{\mathrm{A}}^0) \tag{40}$$

In principle, a nucleus can originate from any random density fluctuations in the metastable homogeneous system and hence the corresponding $\phi_{\mathrm{A}}(\boldsymbol{r})$ is somewhat arbitrary even with a specified $\tilde{M}^{\mathrm{ex}}$. However, the most probable $\phi_{\mathrm{A}}(\boldsymbol{r})$ corresponding to a given $\tilde{M}^{\mathrm{ex}}$ is uniquely determined by solving the SCMFT equations. Hence, the critical nucleus can be obtained from the free energy maximum with respect to $\tilde{M}^{\mathrm{ex}}$. From now on we only consider the critical nucleus.

As we adopt the Schulz chain length distribution, the relation between the number-average chain length and weight-average chain length is $N_0/N_{\mathrm{w}}=k/(k+1)$. The spinodal curve can be determined by

$$(\chi N_0)_{\mathrm{s}}=\frac{1}{2}\left(\frac{1}{\phi_{\mathrm{A}}^0}\frac{k}{k+1}+\frac{1}{\phi_{\mathrm{B}}^0}\right) \tag{41}$$

which is similar to that in monodisperse case except that the N_0 in monodisperse case of polymer A is replaced by the weight-average chain length N_{w}.

Figure 8 shows the χN_0 dependence of the volume fraction at the center of critical nucleus, ϕ_{A} (r = 0). In the case of a monodisperse A/B blends, in the limit of the coexistence curve, $\phi_{\mathrm{A}}(0)$ = 0.84, that is the thermodynamically stable value in coexistence with the bulk phase with $\phi_{\mathrm{A}}^0=0.16$. $\phi_{\mathrm{A}}(0)$ then increases, passing a maximum value, and eventually decreases to $\phi_{\mathrm{A}}^0=0.16$ at the spinodal. The existence of the maximum value is attributed to the higher chemical potential of the metastable bulk with which the nucleus is in coexistence [21]. In the low polydisperse case, e.g., k = 100 and 50, $\phi_{\mathrm{A}}(0)$ also passes a maximum, and in the spinodal limit, it approaches the value of 0.16. In the highly polydisperse case, e.g., k = 10 and 3, $\phi_{\mathrm{A}}(0)$ decreases to 0.16 at a smaller value of χN_0. This is because of the fact that the spinodal point decreases as the polydispersity increases.

The distribution of the volume fraction in the nucleus is different from that in the bulk phase. Figure 9 gives a detailed description of volume fractions of species A. Figure 9 (a) shows the homogeneous volume fraction distribution in the bulk phase, $\phi_{\mathrm{A}}^0(N)$, as a function of N/N_0 for different values

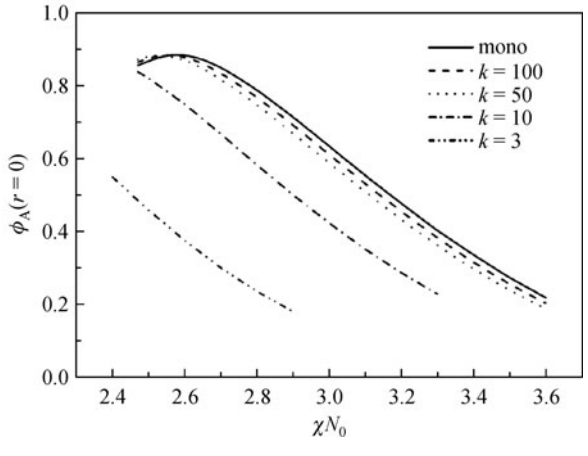

Figure 8 Volume fractions of species A at the centers of critical nuclei, $\phi_{\mathrm{A}}(0)$ as functions of χN_0 for different polydispersity. For a given χN_0, higher polydispersity (small k) leads to lower $\phi_{\mathrm{A}}(0)$. The parameters are taken as $\phi_{\mathrm{A}}^0=0.16$, $N_0=N_{\mathrm{B}}$.

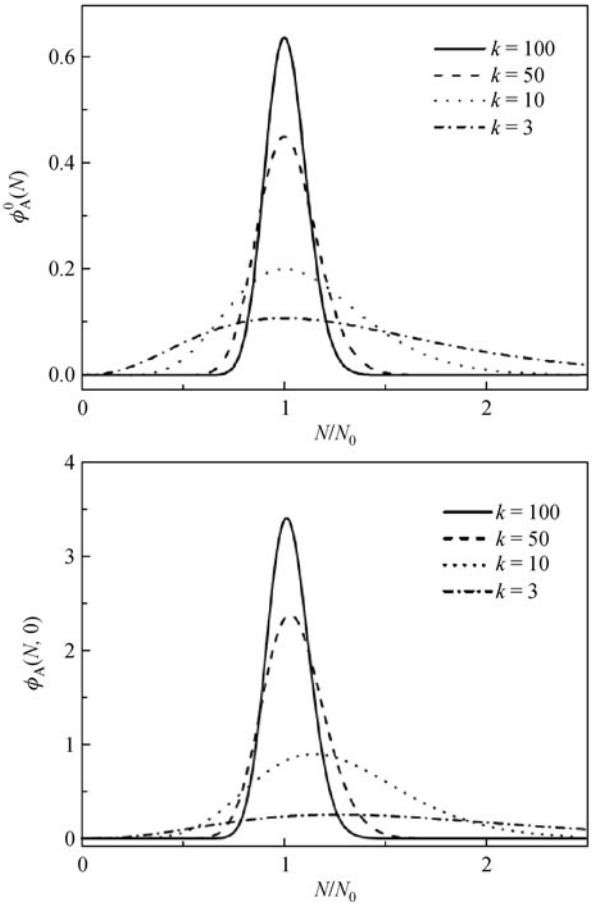

Figure 9 Volume fraction contributions of the polydisperse A species as functions of chain lengths, (N/N_0), for different polydispersity parameters k (a) in homogeneous bulk, and (b) at the centers of critical nuclei. The parameters are taken as $\chi N_0=2.5$, $\phi_{\mathrm{A}}^0=0.16$, and $N_0=N_{\mathrm{B}}$. Higher polydispersity leads to larger N/N_0 for the peak position of $\phi_{\mathrm{A}}(N,0)$.

of k. As chains of different lengths have different abilities to move into the nucleus, the corresponding volume fractions in the nucleus will be different from those in the bulk. Figure 9 (b) shows the volume fraction distribution at the centers of the critical nuclei, $\phi_A(N,0)$, as a function of N/N_0 for different values of k. In the homogeneous bulk phase, the peak of $\phi_A^0(N)$ is at $N = N_0$, as shown in Fig. 9 (a). However, the peak of $\phi_A(N,0)$, which is the volume fraction in the center of critical nucleus, is larger than N_0, and decreases to N_0 at the boundary, where the nucleus and the bulk phase contact. In Fig. 9 (b), these peak positions are at $1.02N_0$, $1.03N_0$, $1.015N_0$, and $1.27N_0$ for k = 100, 50, 10, and 3, respectively. This means that longer chains have stronger tendencies to move to the critical nuclei. Actually, in SCFT, the driving force for the phase separation is proportional to χN. Thus, longer chains have stronger tendencies to separate from the bulk phase and move into the nucleus.

3.4 The self-assembly of diblock copolymers

Block copolymers are formed by chemically connecting strands (or blocks) composed of different monomers. Although the interaction between different blocks tends to drive the system to phase separate, the connectivity of the copolymer chains prevents macroscopic phase separation. As a result, block copolymer systems self-assemble into many complex structures, which have great application potentials. In this subsection, SCMFT is used to study the most basic copolymer system, AB diblock copolymer system.

3.4.1 The phase behaviors of diblock copolymer solutions [8]

Consider a system composed of n_C AB diblock copolymer chains and n_S solvent molecules in a volume V. Each AB chain contains fN A monomers and $(1-f)N$ B monomers. For simplicity, we assume that all monomers have the same volume ρ_0^{-1} as the solvent and the same Kuhn length b. The partition functional of the system can be written as

$$Z = \int \mathcal{D}\{\phi\}\mathcal{D}\{w\}\mathcal{D}\{\eta\}\exp\left(-\mathcal{F}[\{\phi\},\{w\},\{\eta\}]\right) \quad (42)$$

where the free energy functional, $\mathcal{F}[\{\phi\},\{w\},\{\eta\}]$, is given by

$$\begin{aligned}\mathcal{F}[\{\phi\},\{w\},\{\eta\}] &= \frac{1}{2}\sum_{\alpha\neq\beta}\rho_0\chi_{\alpha\beta}\int d\boldsymbol{r}\phi_\alpha(\boldsymbol{r})\phi_\beta(\boldsymbol{r}) - \sum_\alpha \rho_0\int d\boldsymbol{r}\phi_\alpha(\boldsymbol{r})w_\alpha(\boldsymbol{r}) \\ &+\rho_0\int d\boldsymbol{r}\eta(r)\left(\sum_\alpha \phi_\alpha(\boldsymbol{r})-1\right) - \rho_0 V\sum_{p=C,S}\frac{\overline{\phi}_p}{N_p}\ln\frac{z_{0p}eN_p\mathcal{Q}_p}{\rho_0\overline{\phi}_p}\end{aligned} \quad (43)$$

In Eq. (43), α, β = A, B, S; $\chi_{\alpha\beta}$ is the Flory-Huggins parameter, which quantifies the local interaction between each pair of units α and β; $\eta(\boldsymbol{r})$ is the auxiliary field coupled to the incompressible condition; $N_p = N$ or 1 when p = C or S, respectively; z_{0p} is the partition function of component p due to the kinetic energy, which can be regarded as a constant; $\mathcal{Q}_p$ is the partition function of a single molecule of component p.

The set of mean-field equations is as follows:

$$\phi_\alpha(\boldsymbol{r}) = \frac{\overline{\phi}_\alpha}{\mathcal{Q}_\alpha N_\alpha}\int_0^{N_\alpha} ds q_\alpha(\boldsymbol{r},s)q_\alpha^+(\boldsymbol{r},N_\alpha - s) \quad (44)$$

$$w_\alpha(\boldsymbol{r}) = \sum_{\beta\neq\alpha}\chi_{\alpha\beta}\phi_\beta(\boldsymbol{r}) + \eta(\boldsymbol{r}) \quad (45)$$

$$\sum_\alpha \phi_\alpha(\boldsymbol{r}) = 1 \quad (46)$$

Because the equilibrium structure of a diblock copolymer solution is always an ordered phase, the functions of interests here are all periodic functions. Thus it is convenient to use the reciprocal-space method to solve the mean-field equations, in which every function of position can be expanded by a set of orthonormal basis functions, $\{f_i(\boldsymbol{r})\}$, which possesses the symmetry of the structure being considered, e.g.,

$$\phi_\alpha(\boldsymbol{r}) = \sum_{i=1}^{\infty}\phi_i^\alpha f_i(\boldsymbol{r})$$

The expansions of other functions are similar. The unnormalized basis functions can be found from the International Table of Crystallography. By this technique, we need only to find the expansion coefficients, ϕ_i^α, by solving the following equations, which can be derived from Eqs. (44)–(46)

$$\phi_i^\alpha = \frac{\overline{\phi}_\alpha}{\mathcal{Q}_\alpha N_\alpha}\int_0^{N_\alpha} ds\sum_{m,l} q_i^\alpha(s)q_i^{\alpha+}(N_\alpha - s)\Gamma_{iml} \quad (47)$$

$$w_i^\alpha = \sum_{\beta\neq\alpha}\chi_{\alpha\beta}\phi_i^\beta + \eta_i \quad (48)$$

$$\sum_\alpha \phi_i^\alpha = \delta_{i,1} \quad (49)$$

where $\Gamma_{iml} = V^{-1}\int d\boldsymbol{r}f_i(\boldsymbol{r})f_m(\boldsymbol{r})f_l(\boldsymbol{r})$. Note that each of the basis functions is an eigenfunction of the Laplacian operator with eigenvalue λ_i. Then the MDE becomes

$$\frac{\partial q_i^\alpha}{\partial s} = -\sum_m H_{im}q_m^\alpha \quad (50)$$

with

$$H_{im} = \frac{b_\alpha^2}{6}\lambda_i\delta_{im} + \sum_l w_l^\alpha\Gamma_{iml} \quad (51)$$

Here, $b_\alpha = b$ when α = A, B, and $b_\alpha = 0$ when α = S.

After solving these equations by certain iteration technique, the free energy per chain of can be obtained

$$F = \frac{N}{2}\sum_{\alpha\neq\beta}\sum_{i}\chi_{\alpha\beta}\phi_i^{\alpha}\phi_i^{\beta} - \sum_{\alpha}\sum_{i} w_i^{\alpha}\phi_i^{\alpha} - \overline{\phi}_{\mathrm{C}}\ln\mathcal{Q}_{\mathrm{C}} - N\overline{\phi}_{\mathrm{S}}\ln\mathcal{Q}_{\mathrm{S}} + \overline{\phi}_{\mathrm{C}}\ln\overline{\phi}_{\mathrm{C}} + N\overline{\phi}_{\mathrm{S}}\ln\overline{\phi}_{\mathrm{S}} + \mathrm{const.} \quad (52)$$

Then the most stable phase can be determined by comparing the free energies of different structures. Some main results of the calculations are summarized as below.

The phase diagrams $\left(\overline{\phi}_{\mathrm{C}},\chi_{\mathrm{BS}}\right)$ of different compositions and different degrees of copolymerization are presented in Fig. 10. Some general features can be found from the figure. When the copolymer concentration is high, i.e., $\overline{\phi}_{\mathrm{C}} \to 1$, the structure of the system returns to the one of the melt case. Upon dilution, a series of lyotropic structure transitions occur. If the solvent selectivity is high, e.g., $\chi_{\mathrm{BS}} \geqslant 0.7$, the two blocks of the copolymer will swollen up much more unequally. In particular, when the copolymer is asymmetric and the solvent prefers the shorter block, the so-called "inverted" phases, in which the swollen shorter block plus solvent forms the major domain, are formed with the decreasing of $\overline{\phi}_{\mathrm{C}}$. On the other hand, when the solvent becomes weakly selective with decrease χ_{BS}, the possible phase transitions become fewer, and the system finally coincides with the case of neutral solvent as $\chi_{\mathrm{BS}} = \chi_{\mathrm{AS}}$.

Figures 10(a) and (b) are the phase diagrams for two symmetric copolymers with different degrees of copolymerization in solvents of varying selectivity. Both figures display a sequence of $\mathrm{L} \to \mathrm{G_B} \to \mathrm{H_B} \to \mathrm{S_B^{bcc}}$ via dilution in the strongly selective solvent region, while only the transition of L→Dis occurs as the solvent is weakly selective. There is a small existence window of $\mathrm{S_B^{fcc}}$ in Fig. 10(b). We infer that $\mathrm{S_B^{fcc}}$ also emerges in Fig. 10(a) for larger χ_{BS}, although the calculation is too hard to perform there because of the large amount requirement of basis functions. Each order-order transition (OOT) line in these two figures tilts to the right for

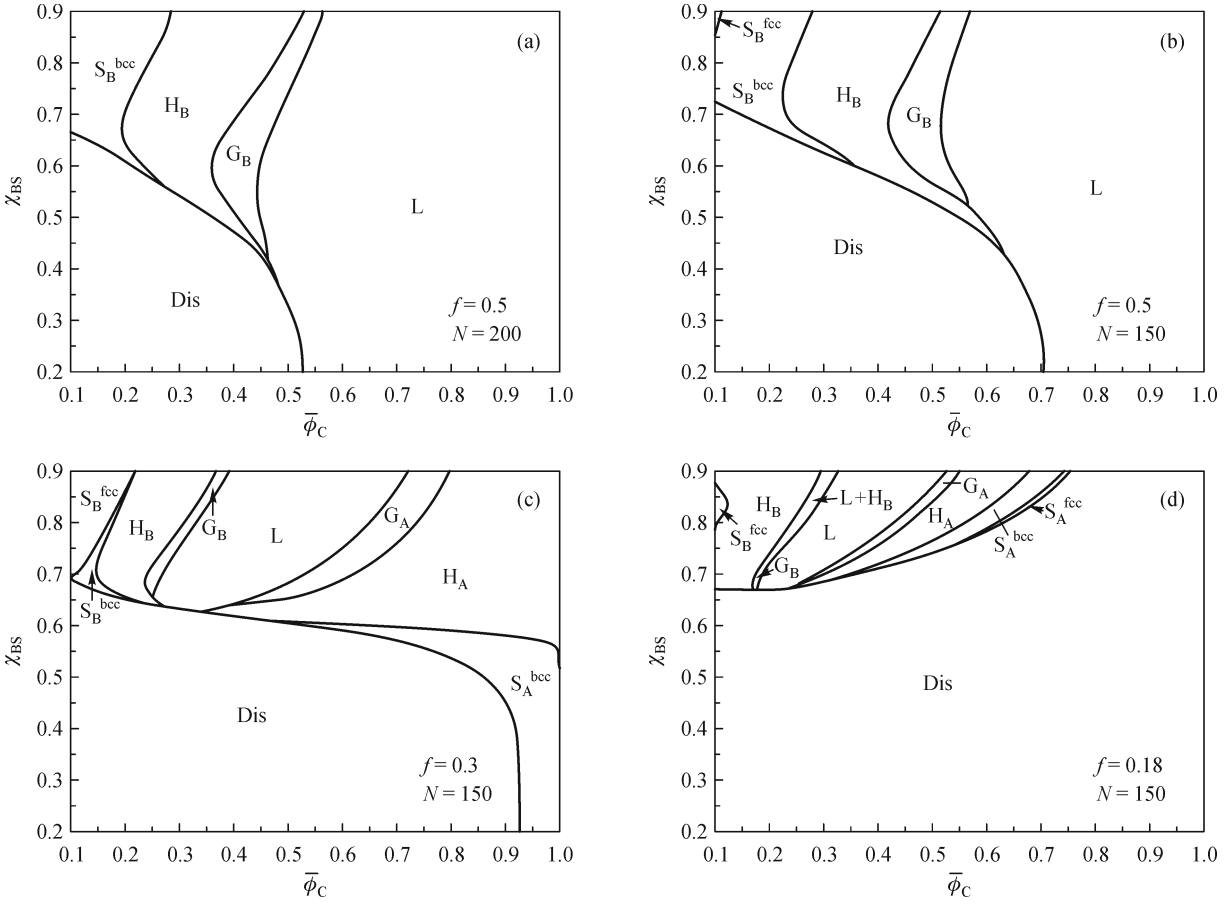

Figure 10 Two-dimensional phase diagram as a function of $\overline{\phi}_{\mathrm{C}}$ and χ_{BS} for a diblock copolymer solution with $\chi_{\mathrm{AB}} = 0.1$, $\chi_{\mathrm{AS}} = 0.2$ and (a) $f = 0.5$, $N = 200$; (b) $f = 0.5$, $N = 150$; (c) $f = 0.3$, $N = 150$; (d) $f = 0.18$, $N = 150$. The ordered phases are denoted as follows: L = lamellae, H = hexagonally packed cylinders, G = gyroid, $\mathrm{S^{bcc}}$ = body-centered cubic spheres, $\mathrm{S^{fcc}}$ = face-centered cubic spheres. Dis = disordered phase. The subscript of each symbol refers to the core composition. The boundary between the regions of $\mathrm{L} + \mathrm{H_B}$ and $\mathrm{G_B}$ in (d) should be considered just as a guide to the eye.

relatively large χ_{BS}, but to the left when χ_{BS} is medium-sized. Thus there is a "reentrant" OOT via varying χ_{BS}. After all, it can be seen that these two figures have quite similar topologies. Only the order-disorder transition (ODT) lines have considerable difference, which is also quantitative. This is a direct reflection of the fact that the variation of N has few effects on OOTs and hence hardly affects the topology of each phase diagram. Thus, we just give the diagrams of $N = 150$ hereafter.

Figure 10(c) is for an asymmetric diblock copolymer, i.e., $f = 0.3$. In this case, the phase behavior becomes more complicated. All possible structures are observed except S_A^{fcc}. Several "reentrant" OOTs occur for the "inverted" structures while the phase line that separates two normal structures just tilts to the right. Moreover, an interesting phenomenon can be observed, i.e., the emergence of the large existence window of S_B^{fcc}. When the composition of the diblock copolymer becomes more asymmetrical, the solution goes into disorder at high copolymer concentration. However, if the solvent has enough selectivity, micelle can form via dilution, and then ordered structures also emerge, as indicated by Fig. 10(d). Particularly, it can be found that the existence window of G_B is substituted by an $L + H_B$ coexistence window when the solvent is strongly selective. This is in agreement with previous experimental observations. The boundary between the regions of $L + H$ and G_B can be determined by the common tangent rule in principle, but it is hard to locate the boundary precisely by numerical methods. Thus the line we put there should be considered just as a guide to the eye.

As can be seen from Figs. 10(b) – (d), the existence window of the "inverted" fcc structure, S_B^{fcc}, becomes larger than that of the "inverted" bcc structure, S_B^{bcc}, when the copolymers become more asymmetric, i.e., the so-called "crew-cut" micelles (with smaller f) favor the fcc structure, while "hairy" micelles (with larger f) favor bcc structure. Also, at low temperatures (large χ_{BS}) the system favors fcc structure, while at high temperatures (small χ_{BS}), especially near the melting line, the system favors bcc structure. A possible mechanism is as follows. Because of the incompressibility, the spherical micelles must fill the whole space. Thus each micelle has to transmute its shape from sphere to that approaching the Wigner-Seitz cell of the ordered structure, which will cause a conformational entropy reduction of each copolymer chain. This kind of transmutation is much harder for the "inverted" micelles than the normal micelles, because the outer part of each "inverted" micelle is composed of the shorter swollen blocks, which have less conformational entropy to adjust than that of the longer chains. Since the Wigner-Seitz cell of fcc lattice (dodecahedron) approaches a sphere closer than that of bcc lattice (truncated octahedron), the "inverted" spherical micelles favor fcc packing when f becomes smaller, as shown in Fig. 10(d).

Generally speaking, most of the phase transitions of a diblock copolymer solution can be comprehended by a simple intuitive geometric consideration, which is based on the relevant concepts of diblock copolymer melts and summarized by Hanley and co-workers as "trajectory approach". The key point is that the addition of a selective solvent always makes the two blocks of the diblock copolymer unequally swollen, leading to changes of the effective composition of the copolymer and the degree of segregation of the system. Thus a sequence of transitions in a copolymer solution is generally corresponding to a tilting trajectory on the phase diagram of a neat copolymer. Take an AB-copolymer of $f = 0.3$ as an example. In the melt state, it will display hexagonally packed cylinders, H_A. With the addition of an A-selective solvent, A-domains must be swollen more than B-domains, which corresponds to an increase of the effective composition. Therefore a sequence of $H_A \rightarrow G_A \rightarrow L \rightarrow G_B \rightarrow H_B \rightarrow S_B^{bcc}$ via dilution can be expected if χ_{BS} is large enough, which is verified in Fig. 10(c). The "reentrant" transitions in Fig. 10, which are obtained by changing χ_{BS}, can be understood by a similar consideration. According to the discussions above, there are two factors to determine the structure of a copolymeric system. One is the degree of segregation, which corresponds to a vertical trajectory on the phase diagram of the melt case. The other is the effective composition of the copolymer, which corresponds to a horizontal trajectory. Changing χ_{BS} will change these two factors simultaneously. However, when $\overline{\phi}_C$ is low but χ_{BS} is high (e.g., the area of $\overline{\phi}_C < 0.5$ and $\chi_{BS} > 0.75$ in Fig. 10(b)), the system is in the strong segregation region where the stable structure of the system is insensitive to the degree of segregation. In this case, the effective composition becomes the dominant factor. Then via decreasing χ_{BS}, the degree of segregation gets lower, and it is necessary to consider both of the two factors to determine the equilibrium phase when χ_{BS} is low enough (e.g., $\chi_{BS} < 0.7$ in Fig. 10(b)). The system can have the same structure in the two limits and so a "reentrant" transition comes.

However, the emergence of the coexistence is not captured in previous discussions. It is well-known that the equilibrium structure of a conformationally symmetric diblock copolymer melt is attributed to the subtle balance of spontaneous curvature and packing frustration. With this consideration, gyroid must exist as a consequence of a compromise between L and H in the case of copolymer melt. However, there can be another kind of compromise, i.e., the coexistence, in a solution. Then the phase behavior of the system is the result of the competition between these two possibilities. Thus, the L +

H coexistence is indeed a consequence that results from the addition of the solvent.

3.4.2 Generic Fourier-space approach [22]

The spectral method provides a complete description of the SCFT equations, which allows high precision calculations of free energies and phase diagrams. For practical reasons, most previous calculations assumed that the symmetry of the ordered phases is known *a priori*. Recently, SCFT calculation using the spectrum method reveals a new continuous phase with space group *Fddd* (the O^{70} phase) [23–25] in diblock copolymers and was indeed observed later in a poly(styrene-b-isoprene) melt. [24] A natural problem is how to predict new structures. Usually the real space method is used to find new phase. However, it always needs to optimize the free energy with respect to the box size to match the natural period and the box size, and hence is hard to release the effects of defects. Recently, a new method to identify this complex based on the spectral method is put forward [22]. The essence of this new approach is to use the full power of the spectral method, in which the symmetry of the ordered phases is not presumed. A generic set of basis functions is generated by the computation box; thus, a spatially varying function is expanded in the form $g(\boldsymbol{r}) = \sum_{\mathrm{G}} g(\boldsymbol{G})\exp(-i\boldsymbol{G}\cdot\boldsymbol{r})$, where the wave vectors $\boldsymbol{G}$ are determined by the size and shape of the box. In the case of a cubic box with length D, the wave vectors are $\boldsymbol{G}_i = (2\pi/D)(h_i, k_i, l_i)$, where $h_i, k_i, l_i = 0, 1, 2 \ldots$. With this generic set of basis functions, in principle the symmetry of the ordered phases will emerge from the solutions. For simplicity in what follows, the centrosymmetric phases restricted, and the expansion takes the form

$$g(\boldsymbol{r}) = \sum_{hkl} g_{hkl}\sqrt{2}\left[-2\pi\left(h\frac{x}{D} + k\frac{y}{D} + l\frac{z}{D}\right)\right] = \sum_{i} g_i\sqrt{2}\cos(\boldsymbol{G}\cdot\boldsymbol{r})$$

Firstly this method is applied to AB diblock copolymers. Up to 294 basis functions are used. A large number of ordered structures emerge from the solutions. In addition to the well-known four equilibrium stable phases (bcc spheres, hexagonal cylinders, gyroids, and lamellae), the solutions include a number of additional structures: an ordered network phase with space group symmetry *Fddd* (the O^{70} phase), a $P6_3mmc$ or $R\bar{3}m$ perforated lamellae, a $Pn3m$ double diamond, and a $P4mm$ phase (which is a network of fourfold connected struts of a minority component forming a tetragonal lattice T^{99}). The generic spectrum method leads to equilibrated lamella, cylinder, gyroid, O^{70}, and sphere phases at the compositions and χ_{AB} values are consistent with the previous work.

In order to demonstrate the predictive power of the new approach, the self assembly in linear frustrated ABC triblock copolymers has been studied. In this system, interaction between the two end blocks is the smallest among the three interactions. To simplify the calculation, the two end block consist the same monomer i.e., $\chi_{\mathrm{CA}}N = \chi_{\mathrm{BC}}N = 35$ and $\chi_{\mathrm{AB}}N = 15$. A large number of ordered phases emerge from the SCFMT calculations (Fig. 11). These structures can be classified into several groups: (i) equilibrium diblock copolymer phases, which are a lamellar (L), gyroid (G), cylinder (C), sphere (S), or disordered phase (D); (ii) core-shell analogs of the G, C, and S phases found in diblock copolymers, in which the middle-block domain forms a shell around the network of one of the end blocks and the other block forms the matrix; (iii) alternating versions of the L, G, C, and S phases, in which the end blocks organize in alternating sublattices and the middle block forms the matrix; (iv) possible combination of the L, G, C, and S phases, including lamellae with cylinders at the interfaces [L + C(I)], lamellae with cylinders inside a domain [L + C(II)], lamellae with spheres at the interfaces [L + S(I)], lamellae with spheres inside a domain [L + S(II)], gyroid with spheres at the interfaces [G + S(I)], and gyroid with spheres inside a domain [G + S(II)]; (v) other decorated phases, such as helical rings on cylinders (C + HEL); (vi) metastable phases such as hexagonally perforated lamellae (HPL).

Figure 12 shows the calculated phase diagrams. A notable feature is that large area of lamellar (L) region exists in the center and near the middle of each binary edge of the phase triangle, which is separated into subregions by decorated phases such as [L + S(II)] near the AB or BC edge and [L + C(I)] and [L + S(I)] near the AC edge. In the subregion at the center of the phase triangle, A, B, and C form well segregated layers — ''three-color'' structure (L3) — while a ''two-color'' structure (L2) in which only two layers can be observed along each of the edges. The region of the G phase near the B corner, which includes the alternating G phase (GA) near the isopleth $f_{\mathrm{A}} = f_{\mathrm{C}}$ and the core-shell version (GCS) near the AB or BC edge, is separated by the G + S phase, in which the sphere is formed by one of the end block. Near the A or C corner, a C + HEL phase is surrounded by the G phase, in which one of the end block forms the cylinder and the middle block forms the helix that winds the cylinder. The C and S phases form continuous arcs across the three corners of the triangle. In the A-rich corner, both phases consist of a C core coated by a B shell immersed in an A matrix, while in the C-rich corner the order is reversed (with A core/B shell/C matrix). In the B-rich corner, alternating C and S phases form near the isopleth $f_{\mathrm{A}} = f_{\mathrm{C}}$, while near the AB and BC edges core-shell versions of the C and S phases are stable. The phase triangle qualitatively agrees with the phase behavior observed

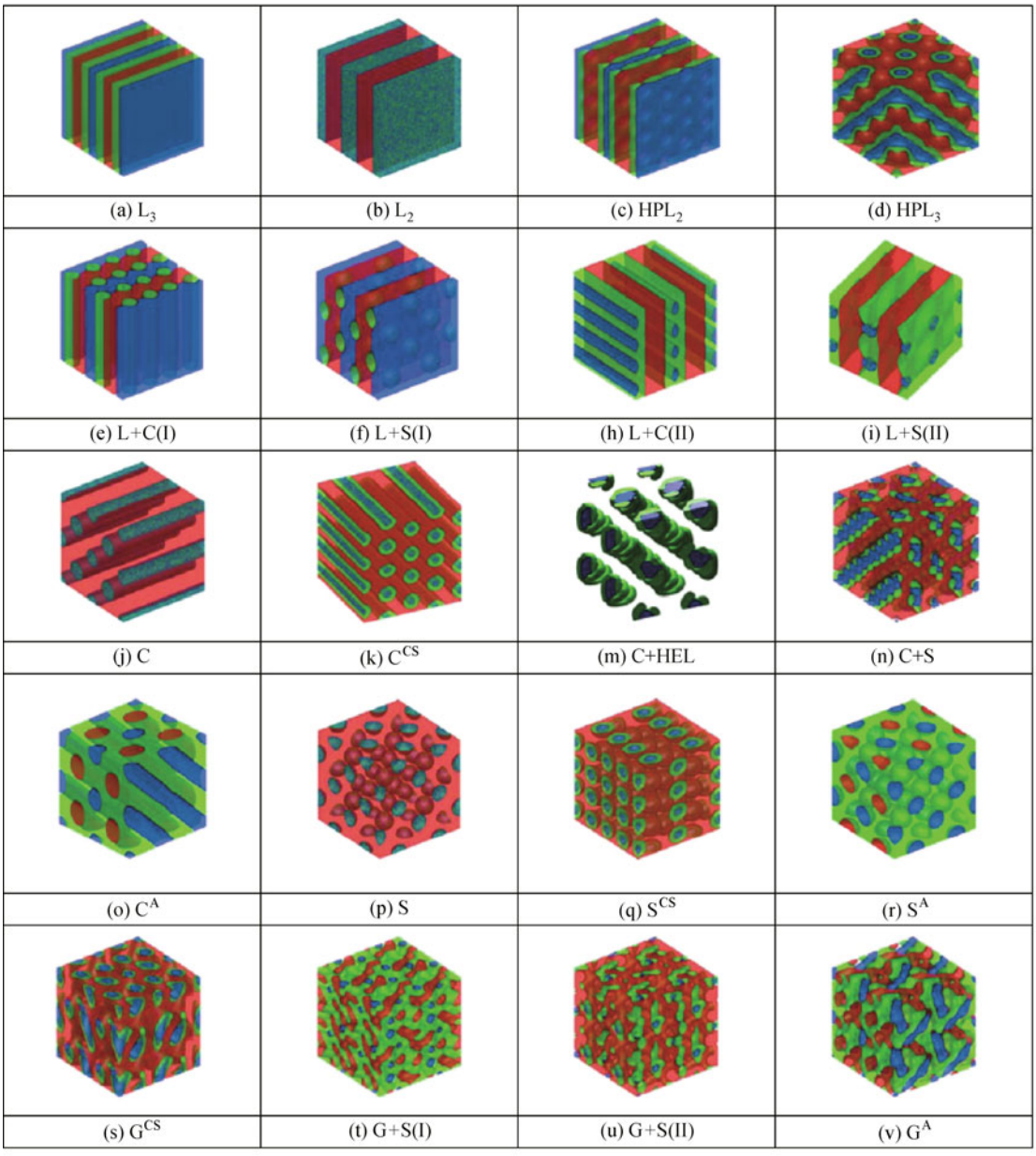

Figure 11 Ordered phases obtained using the generic spectrum approach for model linear ABC triblock copolymers with $\chi_{AB}N = \chi_{BB}N = 35$ and $\chi_{CAN} = 15$. Blue, green, and red represent domains rich in A, B, and C blocks, respectively. Reproduced from Ref. [22], Copyright © 2008 American Physical Society.

for PS-PB-PMMA triblocks experiments. Moreover, the calculated phase sequence L3→ L→C(I)→L + S(I) → L_2 near the isopleth $f_A = f_C$ with decreasing f_B follows the experiment exactly.

4 Gaussian fluctuation theory – applied to confinement systems

In this subsection, we would like to review the applications of Gaussian fluctuation theory [26] to the confinement problem, [27,28] since the Gaussian theory is a natural next-step theoretical development beyond mean-field theory. Within the Gaussian fluctuation theory, the linear stability analyses of morphologies discovered in the SCMFT can be performed and the spinodal lines of these structures can then be constructed theoretically. Furthermore, the nature of phase transitions for the confined diblock copolymer systems can be studied systematically by comparing the spinodal obtained from the Gaussian fluctuation theory to the binodal obtained from the SCMFT.

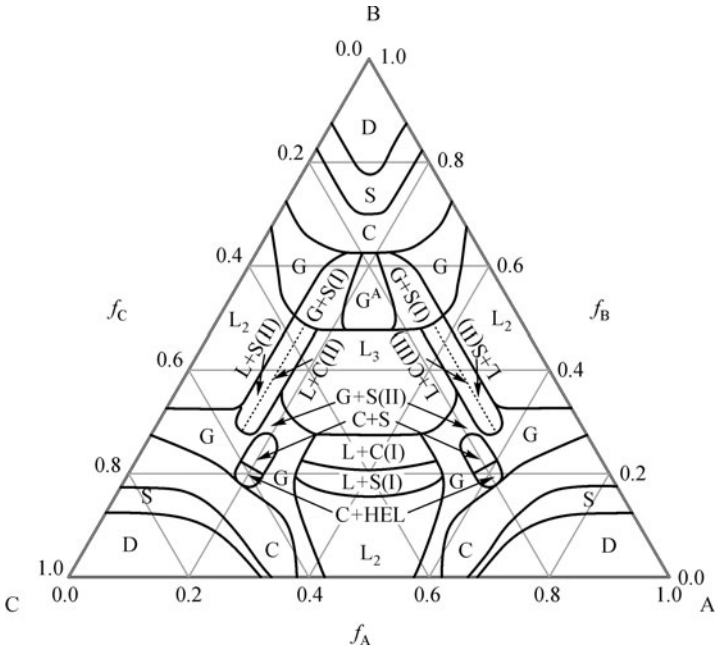

Figure 12 Phase diagram of a model linear ABC triblock copolymer with $\chi_{AC}N = \chi_{BC}N = 35$ and $\chi_{AB}N = 15$. Dotted lines are phase boundaries that are not determined exactly. Reproduced from Ref. [22], Copyright © 2008 American Physical Society.

4.1 Theoretical framework

We give a brief introduction to the framework of Gaussian fluctuation theory as applied to the study of confinement effects in the diblock copolymer melts. The details can be found in Refs. [27,28].

The essential point of this theory is to perform the expansion of the free energy functional around the solution of the SCMFT and then determine the stability (spinodal) of the considered solution by analyzing the Gaussian term in the expansion.

$$F = F^{(0)} + F^{(1)} + F^{(2)} + \cdots \tag{53}$$

Here, F is the free energy functional of the system; $F^{(0)}$ is the mean-field free energy for the considered structure; $F^{(1)}= 0$ since the considered structure as a mean-field solution extremizes the free energy functional; $F^{(2)}$ is the Gaussian term and can be casted in the following form after carrying out the integration of the self-consistent fields in the SCFT resorting to random phase approximation (RPA),

$$F^{(2)}[\delta\phi] = \frac{1}{2}\delta\phi^{+}\cdot(C^{\mathrm{RPA}})^{-1}\cdot\delta\phi \tag{54}$$

where $\delta\phi = \delta\phi_A - \delta\phi_B$; $\delta\phi_\alpha$ is the fluctuation of the density field ϕ_α from the mean-field values for α = A and B; $\delta\phi^+$ is the Hermitian conjugate of $\delta\phi$; $\delta\phi$ and C^{RPA} are generalized matrixes. Because of the incompressibility constraint, the fluctuations in the compositions A and B are not independent. This is the reason why a new collective variable $\delta\phi$ is introduced. The RPA correlation matrix, C^{RPA}, can be constructed in the following way

$$C^{\mathrm{RPA}} = \frac{\rho_0 R_g^3}{N}\left(I - \frac{\chi N}{2}\tilde{C}\right)^{-1}\tilde{C} \tag{55}$$

where ρ_0 is the number density of segments; I is the identity matrix; $\tilde{C} = C - \Delta_1\cdot\Sigma^{-1}\cdot\Delta_2$, in which the operators C, Σ, Δ_1, Δ_2 are combinations of the two-point cumulants $C_{\alpha\beta}$,

$$C = C_{\mathrm{AA}} - C_{\mathrm{AB}} - C_{\mathrm{BA}} + C_{\mathrm{BB}} \tag{56}$$

$$\Sigma = C_{\mathrm{AA}} + C_{\mathrm{AB}} + C_{\mathrm{BA}} + C_{\mathrm{BB}} \tag{57}$$

$$\Delta_1 = C_{\mathrm{AA}} + C_{\mathrm{AB}} - C_{\mathrm{BA}} - C_{\mathrm{BB}} \tag{58}$$

$$\Delta_2 = C_{\mathrm{AA}} - C_{\mathrm{AB}} + C_{\mathrm{BA}} - C_{\mathrm{BB}} \tag{59}$$

In real space, each of $C_{\alpha\beta}$ is an integral over four mean-field propagators

$$\begin{aligned} &C_{\mathrm{AA}}(\boldsymbol{r},\boldsymbol{r}') \\ =&\frac{1}{Q_c}\int_0^{f_A}\mathrm{d}t\int_0^t\mathrm{d}t'\int\mathrm{d}\boldsymbol{r}_1\mathrm{d}\boldsymbol{r}_2\mathrm{d}\boldsymbol{r}_3 \\ &\times[Q_A(\boldsymbol{r}_1,f_A-t|\boldsymbol{r})Q_A(\boldsymbol{r},t-t'|\boldsymbol{r}')Q_A(\boldsymbol{r}',t'|\boldsymbol{r}_2)Q_B(\boldsymbol{r}_2,f_B|\boldsymbol{r}_3) \\ &+Q_A(\boldsymbol{r}_1,f_A-t|\boldsymbol{r}')Q_A(\boldsymbol{r}',t-t'|\boldsymbol{r})Q_A(\boldsymbol{r},t'|\boldsymbol{r}_2)Q_B(\boldsymbol{r}_2,f_B|\boldsymbol{r}_3)] \end{aligned} \tag{60}$$

$$C_{\mathrm{AB}}(\boldsymbol{r},\boldsymbol{r}')$$

$$= \frac{1}{Q_{\mathrm{c}}}\int_0^{f_{\mathrm{A}}}\mathrm{d}t\int_0^{f_{\mathrm{B}}}\mathrm{d}t'\int \mathrm{d}\boldsymbol{r}_1\mathrm{d}\boldsymbol{r}_2\mathrm{d}\boldsymbol{r}_3 \times Q_{\mathrm{A}}(\boldsymbol{r}_1,f_{\mathrm{A}}-t|\boldsymbol{r})Q_{\mathrm{A}}(\boldsymbol{r},t|\boldsymbol{r}_2)Q_{\mathrm{B}}(\boldsymbol{r}_2,t'|\boldsymbol{r}')Q_{\mathrm{B}}(\boldsymbol{r}',f_{\mathrm{B}}-t'|\boldsymbol{r}_3) \tag{61}$$

and C_{BB} and C_{BA} are obtained by exchanging A and B in the above equations, respectively. Q_{c} is the mean-field single-chain partition function which can be obtained from the mean-field propagators,

$$Q_{\mathrm{c}} = \frac{1}{V}\int \mathrm{d}\boldsymbol{r}_1\mathrm{d}\boldsymbol{r}_2\mathrm{d}\boldsymbol{r}_3\; Q_{\mathrm{A}}(\boldsymbol{r}_1,f_{\mathrm{A}}|\boldsymbol{r}_2)Q_{\mathrm{B}}(\boldsymbol{r}_2,f_{\mathrm{B}}|\boldsymbol{r}_3) \tag{62}$$

where $Q_\alpha(\boldsymbol{r},t|\boldsymbol{r}')$ is the mean-field propagator satisfying the modified diffusion equation

$$\frac{\partial Q_\alpha(\boldsymbol{r},t|\boldsymbol{r}')}{\partial t} = -H_\alpha(\boldsymbol{r})Q_\alpha(\boldsymbol{r},t|\boldsymbol{r}') \tag{63}$$

Here, $H_\alpha(\boldsymbol{r}) = -\nabla^2 + \omega_\alpha(\boldsymbol{r})$, here $\omega_\alpha(\boldsymbol{r})$ is the mean field for the considered structure. The eigenequation of the operator $H_\alpha(\boldsymbol{r})$ is

$$H_\alpha(\boldsymbol{r})\psi_n^\alpha(\boldsymbol{r}) = \varepsilon_n^\alpha\psi_n^\alpha(\boldsymbol{r}) \tag{64}$$

As $\{\psi_n^\alpha(\boldsymbol{r})\}$ constitute a complete and orthogonality set, the formulation can be casted into the space spanned by the $\{\psi_n^\alpha(\boldsymbol{r})\}$ set.

In this space, the Gaussian free energy takes the form of

$$F^{(2)}[\delta\phi] = \frac{1}{2}\sum_n\sum_{n'}\delta\phi_n^*(C^{RPA})^{-1}_{n,n'}\delta\phi_{n'} \tag{65}$$

The fluctuation modes in the system can be classified according to the eigenfunctions of $(C^{\mathrm{RPA}})^{-1}$, and the eigenvalues quantify the free energy cost of the Gaussian fluctuations. The most unstable mode, which has the lowest eigenvalue, is called the soft mode of the structure and appears as the most important mode. The condition that the lowest eigenvalue goes to zero determines the spinodal point, and the corresponding eigenfunction characterizes the spatial profile of the most unstable mode.

For the diblock copolymer melts confined by neutral surfaces, it is reasonable to choose the homogeneous structure as the exact mean-field solution. We proceed to determine the spinodal of this homogeneous phase within the framework mentioned above. Because the mean field $\omega_\alpha(\boldsymbol{r})$ is constant for the homogeneous phase, we can take it to be zero by shifting the zero point of the potential. This leads to $H_\alpha(\boldsymbol{r}) = -\nabla^2$. The eigen-problem of the Laplace operator ∇^2 for different boundary conditions, which corresponds to different confined systems, such as systems confined between parallel slabs, cylindrical pores, or spherical pores, is already a well-studied problem in mathematical physics, and hence the basis set $\{\psi_n^\alpha(\boldsymbol{r})\}$ is easy to be obtained. For hard-wall confinements, we can use the free boundary conditions, which is $\nabla\psi_n(r)|_{\mathrm{boundary}} = 0$. We now call the eigenfunction $\psi_n^\alpha(\boldsymbol{r}) = f_n(\boldsymbol{r})$, and the corresponding eigenvalue $\varepsilon_n^a = \lambda_n$. It is straightforward to construct $(C^{\mathrm{RPA}})_{n,n'}$ in this space.

The two-point cumulants are given by

$$C^{\mathrm{AA}}_{n,n'} = 2f_{\mathrm{A}}^2\frac{1-g(\lambda_n f_{\mathrm{A}})}{\lambda_n f_{\mathrm{A}}}\delta_{n,n'} = C_n^{\mathrm{AA}}\delta_{n,n'} \tag{66}$$

$$C^{\mathrm{BB}}_{n,n'} = 2f_{\mathrm{B}}^2\frac{1-g(\lambda_n f_{\mathrm{B}})}{\lambda_n f_{\mathrm{B}}}\delta_{n,n'} = C_n^{\mathrm{BB}}\delta_{n,n'} \tag{67}$$

$$C^{\mathrm{AB}}_{n,n'} = C^{\mathrm{BA}}_{n,n'} = f_{\mathrm{A}}f_{\mathrm{B}}g(\lambda_n f_{\mathrm{A}})g(\lambda_n f_{\mathrm{B}})\delta_{n,n'} = C_n^{\mathrm{AB}}\delta_{n,n'} \tag{68}$$

with $g(x) = (1-\mathrm{e}^{-x})/x$.

Then, the inverse RPA correlation matrix $(C^{\mathrm{RPA}})^{-1}_{n,n'} = (C^{\mathrm{RPA}})_n^{-1}\delta_{n,n'}$ with

$$(C^{\mathrm{RPA}})_n^{-1} = \frac{N}{\rho_0 R_{\mathrm{g}}^3}\left(\tilde{C}_n^{-1} - \frac{\chi N}{2}\right) \tag{69}$$

and

$$\tilde{C}_n = C_n - \frac{(\Delta_1)_n(\Delta_2)_n}{\Sigma_n} \tag{70}$$

with

$$C_n = C_n^{\mathrm{AA}} + C_n^{\mathrm{BB}} - 2C_n^{\mathrm{AB}} \tag{71}$$

$$(\Delta_1)_n = (\Delta_2)_n = C_n^{\mathrm{AA}} - C_n^{\mathrm{BB}} \tag{72}$$

$$\Sigma_n = C_n^{\mathrm{AA}} + C_n^{\mathrm{BB}} + 2C_n^{\mathrm{AB}} \tag{73}$$

Formally, the formula obtained here is the same to the Leibler's result for the bulk melt, except that the energy spectrum changes from continuous to discrete.

We note that, in this case, C^{RPA} turns out to be diagonal in the reciprocal space with $\{f_n(\boldsymbol{r})\}$ as basis set. Physically, this is because that the mean-field structure considered here is homogeneous and translational invariant. This diagonal property implies that the basis $\{f_n(\boldsymbol{r})\}$ is exactly the eigenvector of C^{RPA},

$$\int \mathrm{d}\boldsymbol{r}'\,[C^{\mathrm{RPA}}(\boldsymbol{r},\boldsymbol{r}')]^{-1}f_n(\boldsymbol{r},\boldsymbol{r}') = (C^{\mathrm{RPA}})_n^{-1}f_n(\boldsymbol{r}) \tag{74}$$

Thus, the fluctuation modes for the homogeneous melt confined by neutral surfaces can be classified by $\{f_n(\boldsymbol{r})\}$, and the corresponding eigenvalue $(C^{\mathrm{RPA}})_n^{-1}$ quantifies the Gaussian fluctuation energy cost. The soft mode $f_{n*}(\boldsymbol{r})$ with the lowest energy cost $(C^{\mathrm{RPA}})_{n*}^{-1}$ is the most important fluctuation

mode, which finally destroys the stability of the homogeneous phase. The condition $(C^{\mathrm{RPA}})^{-1}_{n*} = 0$ determines the spinodal. From Eq. (69), we have $(\chi N)_s = 2e_{n*}$, where e_{n*} is the lowest eigenvalue of $\tilde{C}^{-1}$.

4.2 Confinement effects on phase behaviors [27,28]

With the development of nanotechnologies, the confinement effects become important. Both from technological and fundamental point of view, the understanding of the physics in confined system is needed. During the past decades, extensive theoretical studies have been carried out on the confinement effects. Here, we focus only on the phase behaviors of diblock copolymer systems, that serve as a playground for self-assembly. Using the SCMFT, Li and Wickham studied the phase diagram of diblock copolymer melts under cylindrical confinements. Within the two-dimensional calculation, they construct a phase diagram predicting the possible confinement-induced structures [29]. Later, this two-dimensional calculation was improved to the three-dimensional case [30]. Besides, Liang et al. performed the SCMFT studies on the confined diblock copolymers. Particularly, they have been trying to construct a phase diagram of diblock copolymer melts under the spherical confinement [31]. Meanwhile, Yu et al. worked on the cylindrical confined diblock copolymer melts using Monte Carlo simulations [32]. The self-assembly morphologies obtained by the Monte Carlo simulations are consistent with that from SCMFT, and these two methods then form a pair of complementary theoretical tools to look for the confinement-induced morphologies.

Within the framework of Gaussian fluctuation theory, the effects of confinement on the ODT in diblock copolymer melts can be studied systematically. In Figs. 13 and 14, we illustrate the size dependence of the spinodal point $(\chi N)_s$ for the symmetric (f = 0.5) diblock copolymer melts confined between two parallel slabs (Fig. 13) and within a spherical nanopore (Fig. 14), respectively. For the cylindrical confinement, we have similar results as slabs confinement case, and we do not present here to save space. For the slab confinement and the cylindrical confinement, it is observed from the theory that the spinoal of the disordered melts is not affected by the confinement and remains the same as that in the bulk. This result seems to be unexpected. However, it can be well understood by analyzing the soft mode responsible for the linear instability of the disordered structure. From the theory, it is found that the soft mode is a plane wave along the free dimensions, which are the plane parallel to the slabs and the axis direction for the cylindrical pore. Therefore, these fluctuations are free of confinements and cost the same energy as those in the bulk case, and hence lead to the same spinodal as that in the bulk. Since there is no free dimension in the spherical confinements, it can be expected that the spinodal affected by the confinement will be different from that in the bulk. This is exactly what we have observed in the present results. As shown from Fig. 14, the spinodal point of the disordered melt oscillates with the increase of the radius of the spherical pore. This reflects the commensurability between the size of the nanopore and the natural period of

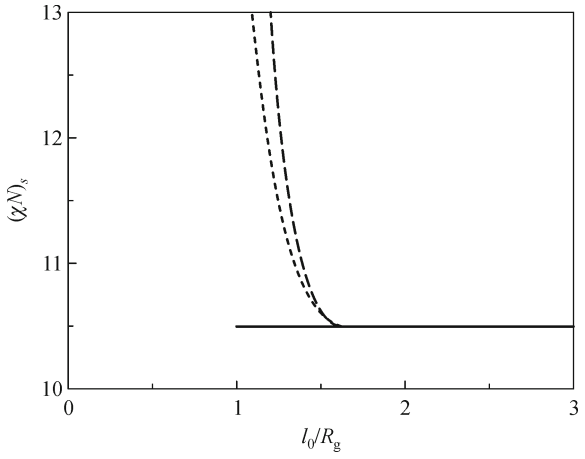

Figure 13 Size dependence of the spinodal point $(\chi N)_s$ for the symmetric (f = 0.5) diblock copolymer melts confined between two parallel slabs with a distance of l_0. The solid line represents the physical spinodal point determined from the most unstable mode with n = 0. The dotted line obtained from the Gaussian fluctuation theory and the dashed line obtained from the Landau-Brazovskii model illustrate the zero point induced by the second-lowest fluctuation mode with n = 1.

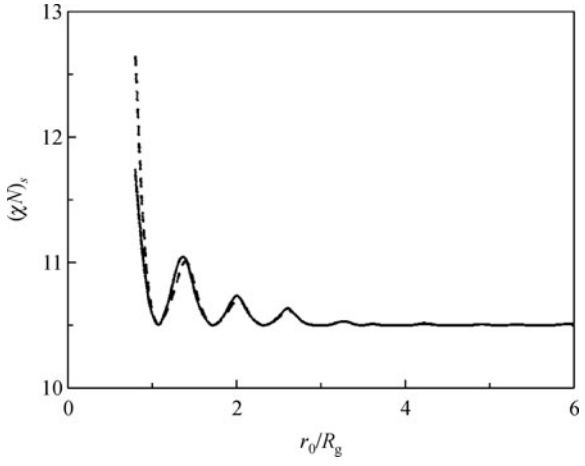

Figure 14 Size dependence of the spinodal point $(\chi N)_s$ for the symmetric (f = 0.5) diblock copolymer melts confined in a spherical pore with the radius of r_0. The solid line and the dashed line are obtained from the Gaussian fluctuation theory and the Landau-Brazovskii model, respectively.

the ordered structure to be formed in the bulk. This is called the structure frustration effect in the confined system. Specifically, when the pore size is almost half-integer times of the natural period of the ordered structure (commensurable), the spinodal is unaffected; when the pore size is uncommensurable to the natural period, the spinodal point $(\chi N)_s$ is increased, signifying that the spinodal of the disordered state is harder to occur due to the higher energy cost to form the deformed ordered structures in the confined space. Also, the confinement effects for the asymmetric ($f \neq 0.5$) diblock copolymer melts have also been studied within the Gaussian fluctuation theory and the phase behavior is similar to the case for the symmetric copolymers.

Since the SCMFT can predict the possible morphologies to be formed in the system and the Gaussian fluctuation theory can analyze the linear stabilities of these structures, it will be promising to combine these two methods and have a full understanding of the phase transitions in the confined system. Bearing this in mind, we choose the symmetric diblock copolymer melts confined between two parallel slabs as a model system, in which we enforce the lamella-forming parallel to the slabs to explore the competition between the structure frustration and the surface interaction. The surface field which acts on one block can be taken as

$$V(\boldsymbol{r}) = -V_0[e^{-x^2/\zeta^2} + e^{-(x-D)^2/\zeta^2}] \tag{75}$$

where V_0 is the strength; D is the separation distance of the slabs; ζ is the decay length of the surface field. The structure evolutions with increase of temperature for a D can be obtained from the SCMFT. In order to identify the OOT and the ODT points in this confined system, we define an order parameter

$$\psi_\varepsilon = \frac{1}{2\varepsilon}\int_{D/2-\varepsilon}^{D/2+\varepsilon} \mathrm{d}x[\phi_\mathrm{A}(x) - f]^2 \tag{76}$$

which characterizes the deviation of the density distribution of one block from that in the homogeneous state.

In Fig. 15, the effect of V_0 on the ODT is illustrated by the order parameter plot for $D = 10R_g$, which is nearly 3 times of the neutral period, and V_0 = 0, 0.1, 1 and 2. For V_0 = 0, an exact ODT can be defined from the order parameter curve, which is the same as that in the bulk, or, χN = 10.5. With the increase of V_0, the transition becomes weaker. Actually, for a large V_0, we cannot define an exact ODT in the finite space. This is due to the fact that the strong preferential surface can induce an oscillating pattern over the whole finite space even when the temperature is high, and the disordered phase cannot be defined effectively. For the case of V_0 = 0, the ODT line from the SCMFT and the spinodal from the Gaussian fluctuation theory are almost the same, and even cannot distinguish from the figure.

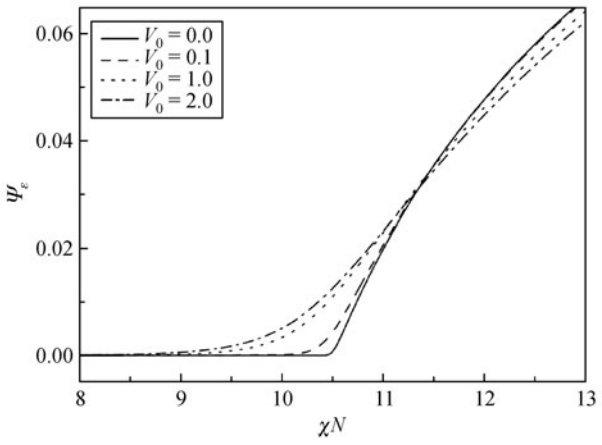

Figure 15 The order parameter, ψ_ε, as a function of χN for the symmetric diblock copolymer melts confined between two slabs with preferential surfaces of different surface strengths of V_0 and the separation distance $D = 10R_g$. The solid, dashed, dotted and dash-dotted lines correspond to the cases of V_0 = 0, 0.1, 1 and 2, respectively.

In Fig. 16, the evolution of order parameter, ψ_ε, with χN is presented for D = 3 L_0 = 9.6 R_g and V_0 = 0.1. The corresponding density pattern is given in Fig. 17. One can find that when D is the integral times of the neutral period, the ODT coincides with the spinodal for the disordered melt. Also, the ODT is continuous in this confinement problem. Meanwhile, with the decrease of the lower temperature, the OOT between different ordered structures happens, which is discontinuous and corresponds that the periodic structure changes from one to another.

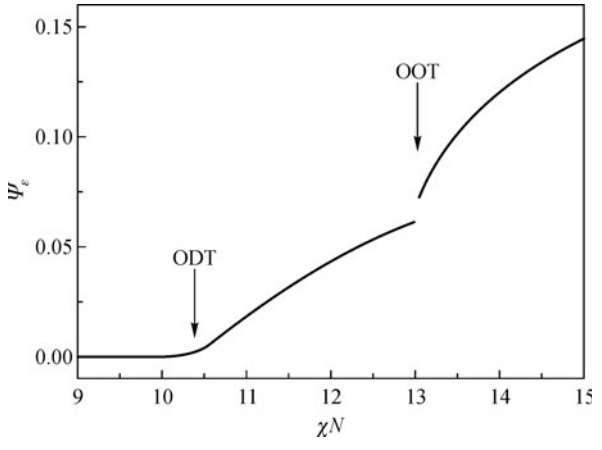

Figure 16 The evolution of the order parameter, ψ_ε, with χN for $D = 3L_0 = 9.6\ R_g$ and V_0 = 0.1. The jump of the order parameter happens around χN = 13.

When D is not the integral times of the neutral period, the ODT is effectively decreased by the surface effect. This reflects the surface-induced ordering phenomena, or, the

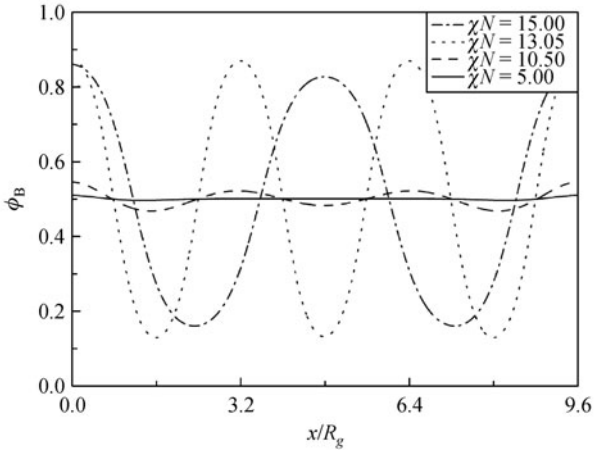

Figure 17 The evolution of the spatial density distribution of block B, φ_B, with χN. $D = 9.6\ R_g$ and $V_0 = 0.1$.

preferential surfaces can induce an oscillating pattern of the density of one block near the surfaces, which will help the disordered melts far from the surfaces to be ordered. This theoretical results have been confirmed experimentally by Kim et al. [33].

5 Summary

In this article we reviewed the most commonly used mesoscopic theory, SCFT. In particular, we focused on the Gaussian chains that are a good model for the flexible polymer system. To demonstrate the power of this theory, several typical systems, including homopolymer and block copolymer, neutral and charged system, polydisperse system and metastable phase, have been investigated. Different kinds of coordinates and numerical methods are chosen to solve the SCFT equations. All of these examples show that the SCFT provides a good connection between the conformation of polymer and the mesoscopic structures. Especially, in the past decades, in collaboration with the field-based simulation, the Gaussian fluctuation theory, the self-consistent Hartree approximation and the Ginzburg-Landau dynamics equation, the SCMFT has served as the basic theoretical method for the experiments and simulations in mesoscopic scale and has promoted a boom of polymer sciences, especially, the self-assembly of block copolymers, the phase separation of polymer blends and the weakly charged polyelectrolytes, etc.

Although SCFT is among the most widely used and successful theories, there are still many problems needed addressing. First, how to solve the MDE efficiently, especially for the semiflexible chains that involves two more degrees of freedom of the orientation. Second, the question how good it is when the SCFT is applied to the dilute or semidilute systems is still unclear. Furthermore, the phenomena involving multiscale, such as crystallization and strongly charged polyelectrolytes, are still hard to be captured.

Acknowledgements We would to thank the other contributors in our group, who are Dr. Hongge Tan, Dr. Shuang Yang and Dr. Shuanhu Qi. Also, we would like to thank Prof. An-Chang Shi for the long-term collaboration. This work was supported by the National Natural Science Foundation of China (NSFC) (Grant Nos. 20973176, 20990234, 50821062, and 20874111), 973 Program of the Ministry of Science and Technology (MOST) (Grant No. 2011CB808502), and the Fundamental Research Funds for the Central Universities.

References

1. de Gennes, P. G., *Scaling Concepts in Polymer Physics*. Ithaca: Cornell University Press, 1979
2. Edwards, S. F., *Proc. Phys. Soc*. **1965**, *85*, 613–624
3. Zhang, P.; Zhang, X.; Li, B.; Wang, Q., *Soft Matter* **2011**, *7*, 4461–4471
4. Helfand, E.; Tagami, Y., *Polym. Lett*. **1971**, *9*, 741–746
5. Helfand, E., *J. Chem. Phys*. **1975**, *62*, 999–1005
6. Shi, A. C., Self-consistent field theory of block copolymers. In: Hamley I. W., ed. Developments in Block Copolymer Science and Technology. New York: John Wiley and Sons, Ltd.: 2004, 265–293
7. Netz, R. R.; Schick, M., *Macromolecules* **1998**, *31*, 5105–5122
8. Suo, T.; Yan, D.; Yang, S.; Shi, A.C., *Macromolecules* **2009**, *42*, 6791–6798
9. Müller, M.; Schmid, F., *Adv. Polym. Sci*. **2005**, *185*, 1–58
10. Yang, S.; Yan, D.; Tan, H., et al., *Phys. Rev. E Stat. Nonlin. Soft Matter Phys*. **2006**, *74*, 041808–1–10
11. Matsen, M. W.; Schick, M., *Phys. Rev. Lett*. **1994**, *72*, 2660–2663
12. Fredrickson, G. H., The Equilibrium Theory of Inhomogeneous Polymers, CLARENDON PRESS, OXFORD, 2006
13. Ceniceros, H. D.; Fredrickson, G. H., *Model. Simul. (Anaheim)* **2004**, *2*, 452–474
14. Thompson, R. B.; Rasmussen, K. Ø.; Lookman, T., *J. Chem. Phys*. **2004**, *120*, 31–34
15. Matsen, M. W., *Eur Phys J E Soft Matter* **2009**, *30*, 361–369
16. Yang, S.; Yan, D.; Shi, A. C., *Macromolecules* **2006**, *39*, 4168–4174
17. Yang, S.; Tan, H.; Yan, D., et al., *Phys. Rev. E Stat. Nonlin. Soft Matter Phys*. **2006**, *75*, 061803–1–7
18. Man, X.; Yang, S.; Yan, D.; Shi, A.C., *Macromolecules* **2008**, *41*, 5451–5456
19. Man, X.; Yan, D., *Macromolecules* **2010**, *43*, 2582–2588
20. Qi, S.; Yan, D., *J. Chem. Phys*. **2008**, *129*, 204902
21. Wood, S. M.; Wang, Z. G., *J. Chem. Phys*. **2002**, *116*, 2289–2300
22. Guo, Z. J.; Zhang, G.; Qiu, F.; Zhang, H.; Yang, Y.; Shi, A. C., *Phys. Rev. Lett*. **2008**, *101*, 028301

23. Tyler, C. A.; Morse, D. C., *Phys. Rev. Lett*. **2005**, *94*, 208302
24. Takenaka, M.; Wakada, T.; Akasaka, S.; Nishitsuji, S.; Saijo, K.; Shimizu, H.; Kim, M. I.; Hasegawa, H., *Macromolecules* **2007**, *40*, 4399–4402
25. Miao, B.; Wickham, R. A., *J. Chem. Phys*. **2008**, *128*, 054902
26. Shi, A-C.; Noolandi, J.; Desai, R. C., *Macromolecules* **1996**, *29*, 6487–6504; Shi, A. C.; Noolandi, J.; Desai, R. C., *Macromolecules* **1997**, *30*, 3242–3255
27. Miao, B.; Yan, D.; Han, C. C.; Shi, A. C., *J. Chem. Phys*. **2006**, *124*, 144902
28. Miao, B.; Yan, D.; Wickham, R. A.; Shi, A. C., *Polymer* **2007**, *48*, 4278–4287
29. Li, W.; Wickham, R. A.; Garbary, R. A., *Macromolecules* **2006**, *39*, 806–811
30. Li, W.; Wickham, R. A., *Macromolecules* **2006**, *39*, 8492–8498
31. Chen, P.; Liang, H.; Shi, A. C., *Macromolecules* **2008**, *41*, 8938–8943
32. Yu, B.; Sun, P.; Chen, T.; Jin, Q.; Ding, D.; Li, B.; Shi, A. C., *Phys. Rev. Lett*. **2006**, *96*, 138306
33. Kim, E.; Ahn, H.; Ryu, D. Y.; Kim, J.; Cho, J., *Macromolecules* **2009**, *42*, 8385–8391